GEOPHYSICS, VOL. 75, NO. 5 (SEPTEMBER-OCTOBER 2010); P. 75A211–75A227, 10 FIGS.
10.1190/1.3463440

Tutorial on seismic interferometry: Part 2 — Underlying theory and new advances

Kees Wapenaar[1], Evert Slob[1], Roel Snieder[2], and Andrew Curtis[3]

ABSTRACT

In the 1990s, the method of time-reversed acoustics was developed. This method exploits the fact that the acoustic wave equation for a lossless medium is invariant for time reversal. When ultrasonic responses recorded by piezoelectric transducers are reversed in time and fed simultaneously as source signals to the transducers, they focus at the position of the original source, even when the medium is very complex. In seismic interferometry the time-reversed responses are not physically sent into the earth, but they are convolved with other measured responses. The effect is essentially the same: The time-reversed signals focus and create a virtual source which radiates waves into the medium that are subsequently recorded by receivers. A mathematical derivation, based on reciprocity theory, formalizes this principle: The cross-correlation of responses at two receivers, integrated over different sources, gives the Green's function emitted by a virtual source at the position of one of the receivers and observed by the other receiver. This Green's function representation for seismic interferometry is based on the assumption that the medium is lossless and nonmoving. Recent developments, circumventing these assumptions, include interferometric representations for attenuating and/or moving media, as well as unified representations for waves and diffusion phenomena, bending waves, quantum mechanical scattering, potential fields, elastodynamic, electromagnetic, poroelastic, and electroseismic waves. Significant improvements in the quality of the retrieved Green's functions have been obtained with interferometry by deconvolution. A trace-by-trace deconvolution process compensates for complex source functions and the attenuation of the medium. Interferometry by multidimensional deconvolution also compensates for the effects of one-sided and/or irregular illumination.

INTRODUCTION

In Part 1, we discussed the basic principles of seismic interferometry (also known as Green's function retrieval[4]) using mainly heuristic arguments. In Part 2, we continue our discussion, starting with an analysis of the relation between seismic interferometry and the field of time-reversed acoustics, pioneered by Fink (1992, 1997). This analysis includes a heuristic discussion of the virtual-source method of Bakulin and Calvert (2004, 2006) and a review of an elegant physical derivation by Derode et al. (2003a, b) of Green's function retrieval by crosscorrelation. After that, we review exact Green's function representations for seismic interferometry in arbitrary inhomogeneous, anisotropic lossless solids (Wapenaar, 2004) and discuss the approximations that lead to the commonly used expressions. We conclude with an overview of recent and new advances, including approaches that account for attenuating and/or nonreciprocal media, methods for obtaining virtual receivers or virtual reflectors, the relationship with imaging theory, and, last but not least, interferometry by deconvolution. The discussion of each of these advances is necessarily brief, but we include many references for further reading.

INTERFEROMETRY AND TIME-REVERSED ACOUSTICS

Review of time-reversed acoustics

In the early 1990s, Mathias Fink and coworkers at the University of Paris VII initiated a new field of research called time-reversed acoustics (Fink, 1992, 1997; Derode et al., 1995; Draeger and Fink,

Manuscript received by the Editor 30 November 2009; published online 14 September 2010.
[1]Delft University of Technology, Department of Geotechnology, Delft, The Netherlands. E-mail: c.p.a.wapenaar@tudelft.nl; e.c.slob@tudelft.nl.
[2]Colorado School of Mines, Center for Wave Phenomena, Golden, Colorado, U.S.A. E-mail: rsnieder@mines.edu.
[3]University of Edinburgh, School of GeoSciences, Edinburgh, U.K. E-mail: andrew.curtis@ed.ac.uk.

[4]By "Green's function," we mean the response of an impulsive point source in the actual medium rather than in a background medium.

1999; Fink and Prada, 2001). Here, we briefly review this research field; in the next sections, we discuss the links with seismic interferometry.

Time-reversed acoustics makes use of the fact that the acoustic wave equation for a lossless acoustic medium is invariant under time reversal (because it only contains even-order time derivatives, i.e., zeroth and second order). This means that when $u(\mathbf{x},t)$ is a solution, then $u(\mathbf{x},-t)$ is a solution as well. Figure 1 illustrates the principle in the context of an ultrasonic experiment (Derode et al., 1995; Fink, 2006). A piezoelectric source at A in Figure 1a emits a short pulse (duration of 1 μs) that propagates through a highly scattering medium (a set of 2000 randomly distributed steel rods with a diameter of 0.8 mm). The transmitted wavefield is received by an array of piezoelectric transducers at B. The received traces (three are shown in Figure 1a) exhibit a long coda (>200 μs) because of multiple scattering between the rods. Next, the traces are reversed in time and simultaneously fed as source signals to the transducers at B (Figure 1b). This time-reversed wavefield propagates through the scattering medium and focuses at the position of the original source. Figure 1c shows the received signal at the original source position; the duration is of the same order as the original signal (~1 μs). Figure 1d shows beam profiles around the source position (amplitudes measured along the x-axis denoted in Figure 1b). The narrow beam is the result of this experiment (back propagation via the scattering medium), whereas the wide beam was obtained when the steel rods were removed.

The resolution is impressive; at the time, the stability of this experiment amazed many researchers. From a numerical experiment, one might expect such good reconstruction; however, when waves have scattered by tens to hundreds of scatterers in a real experiment, the fact that the wavefield refocuses at the original source point is fascinating. Snieder and Scales (1998) have analyzed this phenomenon in detail. In their analysis, they compare wave scattering with particle scattering. They show for their model that, whereas particles behave chaotically after having encountered typically eight scatterers, waves remain stable after 30 or more scatterers. The instability of particle scattering is explained by the fact that particles follow a single trajectory. A small disturbance in initial conditions or scatterer positions causes the particle to follow a completely different trajectory after only a few encounters with the scatterers. Waves, on the other hand, have a finite wavelength and travel along all possible trajectories, visiting all of the scatterers in all possible combinations. Hence, a small perturbation in initial conditions or scatterer positions has a much less dramatic effect for wave scattering than for particle scattering. Consequently, wave-propagation experiments through a strongly scattering medium have a high degree of repeatability. Combined with the invariance of the wave equation for time reversal, this explains the excellent reproduction of the source wavefield after back propagation through the scattering medium.

As a historical side note, the idea of emitting time-reversed signals into a system was proposed and implemented in the 1960s (Parvulescu, 1961, 1995). This was a single-channel method, aiming to compress a complicated response at a detector (for example, in an ocean waveguide) into a single pulse. The method was proposed as a fast alternative to digital crosscorrelation, which, with the computers at that time, cost on the order of 10 days' computation time per correlation for signal lengths typically considered in underwater acoustics (Stewart et al., 1965).

Snieder et al. (2002) and Grêt et al. (2006) exploit the repeatability of acoustic experiments in a method they call *coda wave interferometry* (here, *interferometry* is used in the classical sense). Because the scattering coda is repeatable when an experiment is carried out twice under the same circumstances, any change in the coda between two experiments can be attributed to changes in the medium. As a result of the relatively long duration of the coda, minor time-lapse changes in, for example, the background velocity can be monitored with high accuracy by coda wave interferometry.

Apart from repeatability, another important aspect of time-reversed acoustics is its potential to image beyond the diffraction limit. Consider again the time-reversal experiment in Figure 1. An important effect of the scattering medium between the source at A and the transducer array at B is a widening of the effective aperture angle. In other words, waves that arrive at each receiver include energy from a much wider range of take-off angles from the source location than would be the case without scatterers. A consequence is that time-reversal experiments in strongly scattering media have so-called superresolution properties (de Rosny and Fink, 2002; Lerosey et al., 2007). Hanafy et al. (2009) and Cao et al. (2008) used this property in a seismic time-reversal method to locate trapped miners accurately after a mine collapse.

An essential condition for the stability and high-resolution aspects of time-reversed acoustics is that the time-reversed waves propagate through the same physical medium as in the forward experiment. Here, we see a link between time-reversed acoustics and seismic interferometry. Instead of doing a real reverse-time experiment, in seismic interferometry one convolves forward and time-reversed responses. Because both responses are measured in one and the same physical medium, seismic interferometry has similar stability and high-resolution properties as time-reversed acoustics. This link is made more explicit in the next two sections.

Finally, note that time-reversed acoustics should be distinguished from reverse time migra-

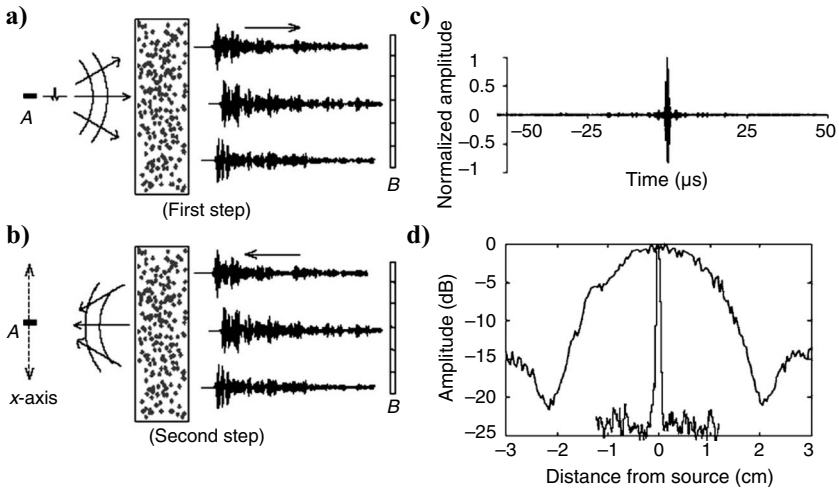

Figure 1. Time-reversed acoustics in a strongly scattering random medium (Derode et al., 1995; Fink, 2006). (a) The source at A emits a short pulse that propagates through the random medium. The scattered waves are recorded by the array at B. (b) The array at B emits the time-reversed signals, which, after back propagation through the random medium, focus at A. (c) The back-propagated response at A. (d) Beam profiles around A.

tion (RTM), such as proposed by McMechan (1982, 1983), Baysal et al. (1983), Whitmore (1983), and Gajewski and Tessmer (2005), in which time-reversed waves are propagated numerically through a macromodel. No matter how much detail one puts into a macromodel, a result such as the one illustrated in Figure 1 can only be obtained when the same physical medium is used in the forward as in the reverse-time experiment. Time-reversed acoustics and reverse time migration serve different purposes. The field of RTM has advanced significantly during the last few years, and contractors and oil companies are now applying the method routinely for depth imaging (Etgen et al., 2009; Zhang and Sun, 2009; Clapp et al., 2010).

Virtual-source method

The method of time-reversed acoustics inspired Rodney Calvert and Andrey Bakulin at Shell to develop what they call the *virtual-source method* (Bakulin and Calvert, 2004, 2006)[5].

In essence, their virtual-source method is an elegant data-driven alternative for model-driven redatuming, similar to Schuster's methods discussed in Part 1 (we point out the differences later). For an acquisition configuration with sources at the surface and receivers in the subsurface — for example, in a near-horizontal borehole (Figure 2) — the reflection response is described as $u(\mathbf{x}_B,\mathbf{x}_S^{(i)},t) = G(\mathbf{x}_B,\mathbf{x}_S^{(i)},t)*s(t)$, where $s(t)$ is the source wavelet and $G(\mathbf{x}_B,\mathbf{x}_S^{(i)},t)$ the Green's function, describing propagation from a point source at $\mathbf{x}_S^{(i)}$ via a target below the borehole to a receiver at $\mathbf{x}_B$ in the borehole (we adopt the notation of Part 1; the asterisk denotes temporal convolution). The downgoing wavefield observed by a downhole receiver at $\mathbf{x}_A$ is given by $u(\mathbf{x}_A,\mathbf{x}_S^{(i)},t) = G(\mathbf{x}_A,\mathbf{x}_S^{(i)},t)*s(t)$. Using source-receiver reciprocity, i.e., $u(\mathbf{x}_A,\mathbf{x}_S^{(i)},t) = u(\mathbf{x}_S^{(i)},\mathbf{x}_A,t)$, this can also be interpreted as the response of a downhole source at $\mathbf{x}_A$, observed by an array of receivers $\mathbf{x}_S^{(i)}$ after propagation through the complex overburden. This response is comparable with the response of the ultrasonic experiment in Figure 1a. Hence, if all traces $u(\mathbf{x}_S^{(i)},\mathbf{x}_A,t)$ would be reversed in time and fed simultaneously as source signals to the sources at $\mathbf{x}_S^{(i)}$, similar as in Figure 1b, the back-propagating wavefield would focus at $\mathbf{x}_A$. Instead of doing this physically, the time-reversed signals are convolved with the reflection responses and subsequently summed over the different source positions at the surface according to

$$C(\mathbf{x}_B,\mathbf{x}_A,t) = \sum_i u(\mathbf{x}_B,\mathbf{x}_S^{(i)},t)*u(\mathbf{x}_A,\mathbf{x}_S^{(i)},-t). \qquad (1)$$

The correlation function $C(\mathbf{x}_B,\mathbf{x}_A,t)$ is interpreted as the response of a virtual downhole source at $\mathbf{x}_A$, measured by a downhole receiver at $\mathbf{x}_B$; hence, $C(\mathbf{x}_B,\mathbf{x}_A,t) \approx G(\mathbf{x}_B,\mathbf{x}_A,t)*S_s(t)$. The wavelet of the virtual source, $S_s(t)$, is the autocorrelation of the wavelet $s(t)$ of the real sources at the acquisition surface. Similar to Schuster's methods, equation 1 can be seen as a form of source redatuming, using a measured version of the redatuming operator, i.e., $u(\mathbf{x}_A,\mathbf{x}_S^{(i)},-t) = G(\mathbf{x}_A,\mathbf{x}_S^{(i)},-t)*s(-t)$.

Whereas in Schuster's methods the emphasis is on aspects such as transforming multiples into primaries, enlarging the illumination area, and interpolating missing traces, the emphasis of Bakulin and Calvert's virtual-source method is on eliminating the propagation distortions of the complex inhomogeneous overburden. Similar to Figure 1, where the time-reversed complex signals at B back propagate through the strongly scattering medium and focus to a short-duration pulse at A, in Bakulin and Calvert's method the sources at the surface are focused to a virtual source in the borehole, compensating for a complex overburden. Similar to the time-reversed acoustics method, the focusing occurs with a time-reversed measured response; hence, the redatuming takes place in the same physical medium as the one in which the data were measured. This distinguishes the virtual-source method from classical redatuming (Berryhill, 1979, 1984) and the common-focal-point (CFP) method (Berkhout, 1997; Berkhout and Verschuur, 2001). Each of these methodologies has its own applications and hence its own right of existence. Classical redatuming and the CFP method are applied to data acquired by sources and receivers at the surface, using as operators either model-based Green's functions (redatuming) or dynamic focusing operators that are aimed to converge iteratively to the Green's functions (CFP method). The virtual-source method uses sources at the surface and receivers in a borehole that directly measure the operators. The idea of using measured Green's functions as redatuming operators may seem simple with hindsight, but the consequences are far reaching. Bakulin et al. (2007) give an impressive overview of the applications in imaging and reservoir monitoring.

A new method for wavelet estimation has been proposed as an interesting corollary of the virtual-source method (Behura, 2007). When the virtual source coincides with a real source at $\mathbf{x}_A$, the response at $\mathbf{x}_B$ from the real source is given by $G(\mathbf{x}_B,\mathbf{x}_A,t)*s(t)$. The virtual-source response, obtained by equation 1, is given by $G(\mathbf{x}_B,\mathbf{x}_A,t)*S_s(t)$, with $S_s(t) = s(t)*s(-t)$. Hence, deconvolution of the virtual-source response by the actual response gives the (time-reversed) wavelet.

Last but not least, we remark that an important difference of equation 1 with the previously discussed expressions for seismic interferometry in Part 1 is the single-sidedness of the correlation function $C(\mathbf{x}_B,\mathbf{x}_A,t) \approx G(\mathbf{x}_B,\mathbf{x}_A,t)*S_s(t)$ [there is no time-reversed term $G(\mathbf{x}_B,\mathbf{x}_A,-t)$]. Moreover, this correlation function is only approximately proportional to the causal Green's function. These are consequences of the anisotropic illumination of the receivers in the borehole, which are primarily illuminated from above. In the "Acoustic Representation" section, we revisit the approximations of one-sided

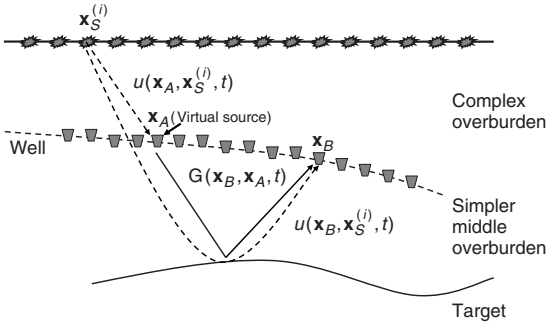

Figure 2. Basic principle of the virtual-source method of Bakulin and Calvert (2004, 2006). Receivers in a borehole record the downgoing wavefield through the complex overburden and the reflected signal from the deeper target. Crosscorrelation and summing over source locations give the reflection response of a virtual source in the borehole, free of overburden distortions.

[5]Recall from part 1 that creating a virtual source is the essence of all seismic interferometry methods; hence, we use the term *virtual source* when appropriate. When it refers to Bakulin and Calvert's method, we mention this explicitly (unless when it is clear from the context).

illumination and indicate various improvements. The most effective improvement is discussed in the "Interferometry by multidimensional deconvolution" section.

Derivation of seismic interferometry from time-reversed acoustics

The virtual-source method, although very elegant, is an intuitive application of time-reversed acoustics. Derode et al. (2003a, b) show more precisely how the principle of Green's function retrieval by crosscorrelation in open systems can be derived from time-reversed acoustics. Their derivation is based entirely on physical arguments and shows that Green's function retrieval (which is equivalent to seismic interferometry), holds for arbitrarily inhomogeneous lossless media, including highly scattering media as shown in Figure 1. Here, we briefly review their arguments, but we replace their notation by that used in Part 1.

Consider a lossless arbitrary inhomogeneous acoustic medium in a homogeneous embedding. In this configuration, we define two points with coordinate vectors $\mathbf{x}_A$ and $\mathbf{x}_B$. Our aim is to show that the acoustic response at $\mathbf{x}_B$ from an impulsive source at $\mathbf{x}_A$ (i.e., the Green's function $G(\mathbf{x}_B,\mathbf{x}_A,t)$) can be obtained by crosscorrelating observations of wavefields at $\mathbf{x}_A$ and $\mathbf{x}_B$ due to sources on a closed surface $\partial\mathbb{D}$ in the homogeneous embedding. The derivation starts by considering another experiment: an impulsive source at $t=0$ at $\mathbf{x}_A$ and receivers at $\mathbf{x}$ on $\partial\mathbb{D}$ (Figure 3a). The response at any point $\mathbf{x}$ on $\partial\mathbb{D}$ is denoted by $G(\mathbf{x},\mathbf{x}_A,t)$. Imagine that we record this response for all $\mathbf{x}$ on $\partial\mathbb{D}$, reverse the time axis, and simultaneously feed these time-reversed functions $G(\mathbf{x},\mathbf{x}_A,-t)$ to sources at all positions $\mathbf{x}$ on $\partial\mathbb{D}$ (Figure 3b). The superposition principle states that the wavefield at any point $\mathbf{x}'$ inside $\partial\mathbb{D}$ due to these sources on $\partial\mathbb{D}$ is given by

$$u(\mathbf{x}',t) \propto \oint_{\partial\mathbb{D}} \underbrace{G(\mathbf{x}',\mathbf{x},t)}_{\text{Propagator}} * \underbrace{G(\mathbf{x},\mathbf{x}_A,-t)}_{\text{Source}} \mathrm{d}^2\mathbf{x}, \qquad (2)$$

where $\propto$ denotes "proportional to." According to equation 2, $G(\mathbf{x}',\mathbf{x},t)$ propagates the source function $G(\mathbf{x},\mathbf{x}_A,-t)$ from $\mathbf{x}$ to $\mathbf{x}'$ and the result is integrated over all sources on $\partial\mathbb{D}$. Because of the invariance of the acoustic wave equation for time-reversal, we know that the wavefield $u(\mathbf{x}',t)$ must focus at $\mathbf{x}'=\mathbf{x}_A$ and $t=0$. This property is the basis of time-reversed acoustics and explains why the focusing in Figure 1 occurs.

Derode et al. (2003a, b) go one step further in their interpretation of equation 2. Because $u(\mathbf{x}',t)$ focuses for $\mathbf{x}'=\mathbf{x}_A$ at $t=0$, the wavefield $u(\mathbf{x}',t)$ for arbitrary $\mathbf{x}'$ and t can be seen as the response of a virtual source at $\mathbf{x}_A$ and $t=0$. This virtual-source response, however, consists of a causal part and an acausal part, according to

$$u(\mathbf{x}',t) = G(\mathbf{x}',\mathbf{x}_A,t) + G(\mathbf{x}',\mathbf{x}_A,-t). \qquad (3)$$

This expression is explained as follows: The wavefield generated by the acausal sources on $\partial\mathbb{D}$ first propagates to all $\mathbf{x}'$ where it gives an acausal contribution; next, it focuses in $\mathbf{x}_A$ at $t=0$. Finally, because the energy focused at that point is not extracted from the system, it must propagate outward again to all $\mathbf{x}'$, giving the causal contribution. The propagation paths from $\mathbf{x}'$ to $\mathbf{x}_A$ are the same as those from $\mathbf{x}_A$ to $\mathbf{x}'$ but are traveled in the opposite direction, which explains the time-symmetric form of $u(\mathbf{x}',t)$.

Combining equations 2 and 3, applying source-receiver reciprocity to $G(\mathbf{x},\mathbf{x}_A,-t)$ in equation 2, and setting $\mathbf{x}'=\mathbf{x}_B$ yields

$$G(\mathbf{x}_B,\mathbf{x}_A,t) + G(\mathbf{x}_B,\mathbf{x}_A,-t) \propto \oint_{\partial\mathbb{D}} G(\mathbf{x}_B,\mathbf{x},t) * G(\mathbf{x}_A,\mathbf{x},-t)\mathrm{d}^2\mathbf{x}. \qquad (4)$$

We recognize the now well-known form of an interferometric relation with, on the left-hand side, the Green's function between $\mathbf{x}_A$ and $\mathbf{x}_B$ plus its time-reversed version and, on the right-hand side, crosscorrelations of wavefield observations at $\mathbf{x}_A$ and $\mathbf{x}_B$, integrated along the sources at $\mathbf{x}$ on $\partial\mathbb{D}$ (Figure 3c). The right-hand side can be reduced to a single crosscorrelation of noise observations in a similar way as discussed in Part 1 (we briefly review this later in the section "Acoustic representation").

Note that equation 4 holds for an arbitrarily inhomogeneous medium inside $\partial\mathbb{D}$; hence, the reconstructed Green's function $G(\mathbf{x}_B,\mathbf{x}_A,t)$ contains the ballistic wave (i.e., the direct wave) as well as the coda resulting from multiple scattering in the inhomogeneous medium. In itself, this is not new because equation 13 in Part 1 is also derived for inhomogeneous media. However, equation 4 is derived directly from the principle of time-reversed acoustics, so it now follows that seismic interferometry has the same favorable stability and resolution properties as time-reversed acoustics. Sens-Schönfelder

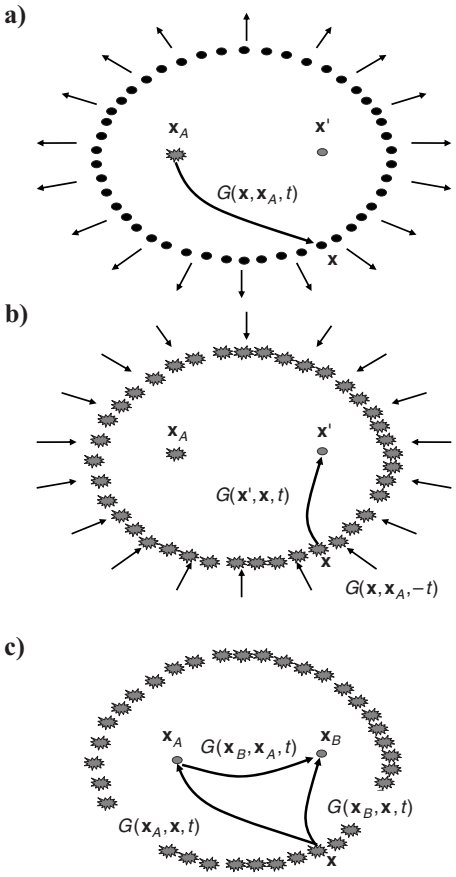

Figure 3. Derivation of Green's function retrieval, using arguments from time-reversed acoustics (Derode et al., 2003a, b). (a) Response of a source at $\mathbf{x}_A$, observed at any $\mathbf{x}$ (the ray represents the full response, including primary and multiple scattering due to inhomogeneities). (b) The time-reversed responses are emitted back into the medium. (c) The response of a virtual source at $\mathbf{x}_A$ can be obtained from the crosscorrelation of observations at two receivers and integration along the sources.

and Wegler (2006) and Brenguier et al. (2008b) exploit the stability properties by applying coda wave interferometry (Snieder et al., 2002) to Green's functions obtained by crosscorrelating noise observations at different seismometers on a volcano. With this method, they can measure velocity variations with an accuracy of 0.1% with a temporal resolution of a single day. Brenguier et al. (2008a) use a similar method to monitor changes in seismic velocity associated with earthquakes near Parkfield, California.

The derivation of Derode et al. (2003a, b) that we have reviewed here is entirely based on elegant physical arguments, but it is not mathematically exact. In the next section, we derive exact expressions and show the approximations that need to be made to arrive at equation 4.

GREEN'S FUNCTION REPRESENTATIONS FOR SEISMIC INTERFEROMETRY

Equations 13 and 14 in Part 1 express the reflection response of a 3D inhomogeneous medium in terms of crosscorrelations of the transmission responses of that medium. We derived these relations in 2002 as a generalization of Claerbout's 1D expressions (equations 8 and 12 in Part 1). The derivation was based on a reciprocity theorem of the correlation type for one-way wavefields. To establish a link with the independently upcoming field of Green's function retrieval, in 2004 we derived the equivalent of these relations in terms of Green's functions for full wavefields (Wapenaar, 2004). The starting point was the Rayleigh-Betti reciprocity theorem for elastodynamic wavefields. Apart from establishing the mentioned link, this derivation has the additional advantage that the inherent approximations of the one-way reciprocity theorem of the correlation type are circumvented (or at least postponed to a later stage in the derivation).

Elastodynamic representation

Here, we briefly review our derivation of the elastodynamic Green's function representation for interferometry and discuss the connection with the methods discussed in the previous section and in Part 1. Consider an arbitrarily heterogeneous and anisotropic lossless solid medium with stiffness $c_{ijkl}(\mathbf{x})$ and mass density $\rho(\mathbf{x})$. In this medium, an external force distribution $f_i(\mathbf{x},t)$ generates an elastodynamic wavefield, characterized by stress tensor $\tau_{ij}(\mathbf{x},t)$ and particle velocity $v_i(\mathbf{x},t)$. The Fourier transforms of these time-dependent quantities are defined via

$$\hat{f}(\omega) = \int_{-\infty}^{\infty} f(t)\exp(-j\omega t)\mathrm{d}t, \tag{5}$$

where ω is the angular frequency and j is the imaginary unit. In the space-frequency domain, the stress-strain relation reads $j\omega\hat{\tau}_{ij} - c_{ijkl}\partial_l\hat{v}_k = 0$ and the equation of motion is $j\omega\rho\hat{v}_i - \partial_j\hat{\tau}_{ij} = \hat{f}_i$. The operator ∂_j denotes the partial derivative in the x_j-direction, and Einstein's summation convention applies to repeated subscripts.

In the following, we consider two independent elastodynamic states (i.e., sources and wavefields) distinguished by subscripts A and B. For an arbitrary spatial domain $\mathbb{D}$ enclosed by boundary $\partial\mathbb{D}$ with outward-pointing normal $\mathbf{n} = (n_1,n_2,n_3)$, the Rayleigh-Betti reciprocity theorem that relates these two states is given by

$$\int_{\mathbb{D}} \{\hat{f}_{i,A}\hat{v}_{i,B} - \hat{v}_{i,A}\hat{f}_{i,B}\}\mathrm{d}^3\mathbf{x} = \oint_{\partial\mathbb{D}} \{\hat{v}_{i,A}\hat{\tau}_{ij,B} - \hat{\tau}_{ij,A}\hat{v}_{i,B}\}n_j\mathrm{d}^2\mathbf{x} \tag{6}$$

(Knopoff and Gangi, 1959; de Hoop, 1966; Aki and Richards, 1980). This theorem is also known as a reciprocity theorem of the convolution type because all products in the frequency domain, such as $\hat{v}_{i,A}\hat{\tau}_{ij,B}$, correspond to convolutions in the time domain.

Similarly to the acoustic situation, we can apply the principle of time-reversal invariance for elastic waves in a lossless medium (Bojarski, 1983). Time reversal corresponds to complex conjugation in the frequency domain. Hence, when stress tensor $\hat{\tau}_{ij}$ and particle velocity $\hat{v}_i$ are solutions of the stress-strain relation and the equation of motion with source term $\hat{f}_i$, then $\hat{\tau}^*_{ij}$ and $-\hat{v}^*_i$ obey the same equations with source term $\hat{f}^*_i$ (the negative sign in $-\hat{v}^*_i$ comes from the replacement $(j\omega)^* = -j\omega$ in the equation of motion). Making these substitutions for state A, we obtain

$$\int_{\mathbb{D}} \{\hat{f}^*_{i,A}\hat{v}_{i,B} + \hat{v}^*_{i,A}\hat{f}_{i,B}\}\mathrm{d}^3\mathbf{x} = \oint_{\partial\mathbb{D}} \{-\hat{v}^*_{i,A}\hat{\tau}_{ij,B} - \hat{\tau}^*_{ij,A}\hat{v}_{i,B}\}n_j\mathrm{d}^2\mathbf{x}. \tag{7}$$

This is an elastic reciprocity theorem of the correlation type because products such as $\hat{v}^*_{i,A}\hat{\tau}_{ij,B}$ correspond to correlations in the time domain.

Next, we replace the wavefields in both states in equation 7 by Green's functions. This means that we replace the force distributions by unidirectional impulsive point forces in both states, according to $f_{i,A}(\mathbf{x},t) = \delta(\mathbf{x}-\mathbf{x}_A)\delta(t)\delta_{ip}$ and $f_{i,B}(\mathbf{x},t) = \delta(\mathbf{x}-\mathbf{x}_B)\delta(t)\delta_{iq}$ in the time domain or $\hat{f}_{i,A}(\mathbf{x},\omega) = \delta(\mathbf{x}-\mathbf{x}_A)\delta_{ip}$ and $\hat{f}_{i,B}(\mathbf{x},\omega) = \delta(\mathbf{x}-\mathbf{x}_B)\delta_{iq}$ in the frequency domain, with $\mathbf{x}_A$ and $\mathbf{x}_B$ in $\mathbb{D}$ and where indices p and q denote the directions of the applied forces. Accordingly, for the particle velocities, we substitute $\hat{v}_{i,A}(\mathbf{x},\omega) = \hat{G}_{ip}(\mathbf{x},\mathbf{x}_A,\omega)$ and $\hat{v}_{i,B}(\mathbf{x},\omega) = \hat{G}_{iq}(\mathbf{x},\mathbf{x}_B,\omega)$, respectively. Here, $\hat{G}_{ip}(\mathbf{x},\mathbf{x}_A,\omega)$ represents the i component of the particle velocity at $\mathbf{x}$ due to a unit force source in the p direction at $\mathbf{x}_A$, etc. Substituting these sources and Green's functions into equation 7, using the stress-strain relation and source-receiver reciprocity (i.e., $\hat{G}_{ip}(\mathbf{x},\mathbf{x}_A,\omega) = \hat{G}_{pi}(\mathbf{x}_A,\mathbf{x},\omega)$), gives

$$\hat{G}_{qp}(\mathbf{x}_B,\mathbf{x}_A,\omega) + \hat{G}^*_{qp}(\mathbf{x}_B,\mathbf{x}_A,\omega) = -\oint_{\partial\mathbb{D}} \frac{c_{ijkl}(\mathbf{x})}{j\omega}((\partial_l\hat{G}_{qk}(\mathbf{x}_B,\mathbf{x},\omega))\hat{G}^*_{pi}(\mathbf{x}_A,\mathbf{x},\omega) - \hat{G}_{qi}(\mathbf{x}_B,\mathbf{x},\omega)\partial_l\hat{G}^*_{pk}(\mathbf{x}_A,\mathbf{x},\omega))n_j\mathrm{d}^2\mathbf{x}. \tag{8}$$

In the time domain,

$$\partial_t\{G_{qp}(\mathbf{x}_B,\mathbf{x}_A,t) + G_{qp}(\mathbf{x}_B,\mathbf{x}_A,-t)\} = -\oint_{\partial\mathbb{D}} c_{ijkl}(\mathbf{x})(\partial_l G_{qk}(\mathbf{x}_B,\mathbf{x},t) * G_{pi}(\mathbf{x}_A,\mathbf{x},-t) - G_{qi}(\mathbf{x}_B,\mathbf{x},t) * \partial_l G_{pk}(\mathbf{x}_A,\mathbf{x},-t))n_j\mathrm{d}^2\mathbf{x}. \tag{9}$$

Note that this representation has a similar form as many of the expressions we have encountered before. It is an exact representation

for the Green's function between $\mathbf{x}_A$ and $\mathbf{x}_B$ plus its time-reversed version, expressed in terms of crosscorrelations of wavefield observations at $\mathbf{x}_A$ and $\mathbf{x}_B$, integrated along the sources at $\mathbf{x}$ on $\partial\mathbb{D}$. It holds for an arbitrarily inhomogeneous anisotropic medium (inside as well as outside $\partial\mathbb{D}$), and the closed boundary $\partial\mathbb{D}$ containing the sources of the Green's functions may have any shape. When a part $\partial\mathbb{D}_0$ of the boundary is a stress-free surface, as in Figure 4, then the integrand of the right-hand side of equation 7 is zero on $\partial\mathbb{D}_0$. Consequently, the boundary integral in equation 9 need only be evaluated over the remaining part $\partial\mathbb{D}_1$ (meaning that sources can be restricted to that part of the boundary). Note that equation 9 still holds in the limiting case in which $\mathbf{x}_A$ and $\mathbf{x}_B$ lie at the free surface. In that case, the Green's functions on the left-hand side have a traction source at $\mathbf{x}_A$ (Wapenaar and Fokkema, 2006).

An important difference with earlier expressions is that the right-hand side of representation 9 contains a combination of two terms, where each of the terms is a crosscorrelation of Green's functions with different types of sources at $\mathbf{x}$ (e.g., the operator ∂_l in $\partial_l G_{qk}(\mathbf{x}_B,\mathbf{x},t)$ is a differentiation with respect to x_l, which changes the character of the source at $\mathbf{x}$ of this Green's function). For modeling applications, this is not a problem because any type of source can be defined in modeling. Van Manen et al. (2006, 2007) use equation 9 for what they call *interferometric modeling*. They model the response of different types of sources on a boundary and save the responses for all possible receiver positions in the volume enclosed by the boundary. Next, they apply equation 9 to obtain the responses of all possible source positions in that volume. Hence, for the cost of modeling responses of sources on a boundary (and calculating many crosscorrelations), they obtain responses of sources throughout a volume. This approach can be very useful for nonlinear inversion schemes, where, in each iteration, Green's functions for sources in a volume are required.

The requirement of correlating responses of different types of sources makes equation 9 in its present form less practical for application in seismic interferometry. This is particularly true for passive data, where one must rely on the availability of natural sources. To accommodate this situation, equation 9 can be modified (Wapenaar and Fokkema, 2006). Here, we only indicate the main steps. Using a high-frequency approximation, assuming the medium outside $\partial\mathbb{D}$ is homogeneous and isotropic, the sources can be decomposed into P- and S-wave sources and their derivatives in the direction of the normal on $\partial\mathbb{D}$. These derivatives can be approximated, leading to a simplified version of equation 9 in which only crosscorrelations of Green's functions with the same source type occur. This approximation is accurate when $\partial\mathbb{D}$ is a sphere with large radius. It can also be used for arbitrary surfaces $\partial\mathbb{D}$ but at the expense of amplitude errors. Because the approximation does not affect the phase, it is usually considered acceptable for seismic interferometry. Finally, when the sources are mutually uncorrelated noise sources for P- and S-waves on $\partial\mathbb{D}$, equation 9 reduces to

$$\{G_{qp}(\mathbf{x}_B,\mathbf{x}_A,t) + G_{qp}(\mathbf{x}_B,\mathbf{x}_A,-t)\} * S_N(t) \approx \frac{2}{\rho c_P}\langle v_q(\mathbf{x}_B,t) * v_p(\mathbf{x}_A,-t)\rangle, \quad (10)$$

where $v_p(\mathbf{x}_A,t)$ and $v_q(\mathbf{x}_B,t)$ are the p and q components of the particle velocity of the noise responses at $\mathbf{x}_A$ and $\mathbf{x}_B$, respectively; $S_N(t)$ is the autocorrelation of the noise; and c_P is the P-wave propagation velocity of the homogeneous medium outside $\partial\mathbb{D}$. For the configuration of Figure 4, the Green's function $G_{qp}(\mathbf{x}_B,\mathbf{x}_A,t)$ retrieved by equation 10 contains the surface waves between $\mathbf{x}_A$ and $\mathbf{x}_B$ as well as the reflected and refracted waves, assuming the noise sources are well distributed over the source boundary $\partial\mathbb{D}_1$ in the half-space below the free surface. In practice, equation 10 is used either for surface-wave or for reflected-wave interferometry.

For surface-wave interferometry, the sources at and close to the surface typically give the most relevant contributions — say, the sources above the dashed line in Figure 4. In our earlier, more intuitive discussions on direct-wave interferometry in Part 1, we consider the fundamental surface-wave mode as an approximate solution of a 2D wave equation in the horizontal plane and argue that the Green's function of this fundamental mode can be extracted by crosscorrelating ambient noise. Equation 10 is a corollary of the exact 3D representation 9 and thus accounts not only for the fundamental mode of the direct surface wave but also for higher-order modes as well as for scattered surface waves. Halliday and Curtis (2008) carefully analyze the contributions of the different sources to the retrieval of surface waves. They show that when only sources at the surface are available, there is strong spurious interference between higher modes and the fundamental mode, whereas the presence of sources at depth (between the free surface and, say, the dashed line in Figure 4) enables the correct recovery of all modes independently. Nevertheless, they show that it is possible to obtain the latter result using only surface sources if modes are separated before crosscorrelation, are correlated separately, and are reassembled thereafter. Kimman and Trampert (2010) show that the spurious interference is also suppressed when the surface sources are very far away or organized in a band. Halliday and Curtis (2009b) analyze the requirements in terms of source distribution for the retrieval of scattered surface waves. Halliday et al. (2010a) use the acquired insights to remove scattered surface waves (ground roll) from seismic shot records (Figure 5).

For reflected-wave interferometry, the deeper situated sources (typically those below the dashed line in Figure 4) give the main contributions. This is in agreement with our discussion on the retrieval of the 3D reflection response from transmission data, for which we consider a configuration with sources in the lower half-space (Figure 12, Part 1). For this configuration, Green's function representations

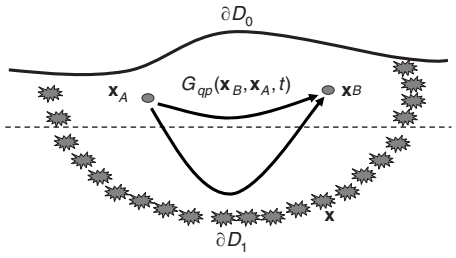

Figure 4. Configuration for elastodynamic Green's function retrieval (the rays represent the full response, including primary and multiple scattering as well as mode conversion due to inhomogeneities). In this configuration, a part of the closed boundary is a free surface ($\partial\mathbb{D}_0$), so sources are only required on the remaining part of the boundary ($\partial\mathbb{D}_1$). The shallow sources (say, above the dashed line) are mainly responsible for retrieving the surface waves and the direct and shallowly refracted waves in $G_{qp}(\mathbf{x}_B,\mathbf{x}_A,t)$, whereas the deeper sources mainly contribute to the retrieval of the reflected waves in $G_{qp}(\mathbf{x}_B,\mathbf{x}_A,t)$.

9 and 10 can be seen as alternatives for reflection representations 13 and 14 in Part 1, generalized for an anisotropic solid medium.

Acoustic representation

Starting with Rayleigh's reciprocity theorem (Rayleigh, 1878; de Hoop, 1988; Fokkema and van den Berg, 1993) and the principle of time-reversal invariance (Bojarski, 1983; Fink, 1992), we obtain the acoustic analogue of equation 8 according to

$$\hat{G}(\mathbf{x}_B,\mathbf{x}_A,\omega) + \hat{G}^*(\mathbf{x}_B,\mathbf{x}_A,\omega) = -\oint_{\partial\mathbb{D}} \frac{1}{j\omega\rho(\mathbf{x})}((\partial_i\hat{G}(\mathbf{x}_B,\mathbf{x},\omega))\hat{G}^*(\mathbf{x}_A,\mathbf{x},\omega) - \hat{G}(\mathbf{x}_B,\mathbf{x},\omega)\partial_i\hat{G}^*(\mathbf{x}_A,\mathbf{x},\omega))n_i\mathrm{d}^2\mathbf{x} \quad (11)$$

(van Manen et al., 2005; Wapenaar et al., 2005). Here, $\hat{G}(\mathbf{x}_A,\mathbf{x},\omega) = \hat{G}(\mathbf{x},\mathbf{x}_A,\omega)$ is a solution of the wave equation

$$\rho\partial_i(\rho^{-1}\partial_i\hat{G}) + \left(\frac{\omega^2}{c^2}\right)\hat{G} = -j\omega\rho\delta(\mathbf{x}-\mathbf{x}_A), \quad (12)$$

for an arbitrarily inhomogeneous lossless fluid medium with propagation velocity $c = c(\mathbf{x})$ and mass density $\rho = \rho(\mathbf{x})$.

Before we discuss its use in seismic interferometry, we remark that equation 11 has been used in almost the same form in optical holography (Porter, 1970), seismic migration (Esmersoy and Oristaglio, 1988), and acoustic inverse scattering (Oristaglio, 1989) (except that in those papers the Green's functions are defined without the factor $j\omega\rho$ in the right-hand side of equation 12, leading to a somewhat different form of equation 11). In imaging and inversion literature, $\hat{G}(\mathbf{x}_B,\mathbf{x}_A,\omega) + \hat{G}^*(\mathbf{x}_B,\mathbf{x}_A,\omega)$ is also called the homogeneous Green's function because $\hat{G}_h(\mathbf{x},\mathbf{x}_A,\omega) = \hat{G}(\mathbf{x},\mathbf{x}_A,\omega) + \hat{G}^*(\mathbf{x},\mathbf{x}_A,\omega)$ obeys the homogeneous wave equation

$$\rho\partial_i(\rho^{-1}\partial_i\hat{G}_h) + \left(\frac{\omega^2}{c^2}\right)\hat{G}_h = 0 \quad (13)$$

("homogeneous" means source free in this context). The homogeneous Green's function $\hat{G}_h(\mathbf{x},\mathbf{x}_A,\omega)$ can also be seen as the resolution function of the imaging integral. For a homogeneous medium, it is given by

$$\hat{G}_h(\mathbf{x},\mathbf{x}_A,\omega) = j\omega\rho\left(\frac{\mathrm{e}^{-jkr}}{4\pi r} - \frac{\mathrm{e}^{jkr}}{4\pi r}\right) = \omega\rho\frac{\sin(kr)}{2\pi r}, \quad (14)$$

with $k = \omega/c$ and $r = |\mathbf{x}-\mathbf{x}_A|$. This function has its maximum for $r\to 0$, where the amplitude is equal to $\omega^2\rho/2\pi c$. The width of the main lobe (measured at the zero crossings) is equal to the wavelength $\lambda = 2\pi/k$. For a further discussion on the relation between seismic interferometry and the migration resolution integral, see van Manen et al. (2006), Thorbecke and Wapenaar (2007), and Halliday and Curtis (2010).

Consider again the acoustic Green's function representation for seismic interferometry (equation 11). Note that in comparison with, for example, equation 4, the right-hand side contains a combination of two terms, where each term is a crosscorrelation of Green's functions with different types of sources (monopoles and dipoles) at $\mathbf{x}$. Here, we discuss in more detail how we can combine the two correlation products in equation 11 into a single term. To this end, we assume that the medium outside $\partial\mathbb{D}$ is homogeneous, with constant propagation velocity c and mass density ρ. In the high-frequency regime, the derivatives of the Green's functions can be approximated by multiplying each constituent (direct wave, scattered wave, etc.) by $-jk|\cos\alpha|$, where α is the angle between the relevant ray and the normal on $\partial\mathbb{D}$. The main contributions to the integral in equation 11 come from stationary points on $\partial\mathbb{D}$. At those points, the ray angles for both Green's functions are identical (see Appendix A of Part 1). This implies that the contributions of the two terms under the integral in equation 11 are approximately equal (but opposite in sign); hence,

$$\hat{G}(\mathbf{x}_B,\mathbf{x}_A,\omega) + \hat{G}^*(\mathbf{x}_B,\mathbf{x}_A,\omega) \approx -\frac{2}{j\omega\rho}\oint_{\partial\mathbb{D}} (n_i\partial_i\hat{G}(\mathbf{x}_B,\mathbf{x},\omega))\hat{G}^*(\mathbf{x}_A,\mathbf{x},\omega)\mathrm{d}^2\mathbf{x}. \quad (15)$$

The integrand contains a single crosscorrelation product of dipole and monopole source responses. When only monopole responses are available, the operation $n_i\partial_i$ can be replaced by a pseudodifferential operator acting along $\partial\mathbb{D}$ or by multiplications with $-jk|\cos\alpha|$ at the stationary points when the ray angles are known. Hence, for controlled-source interferometry, in which case the source positions are known and $\partial\mathbb{D}$ is a smooth surface, equation 15 is a useful expression.

In passive interferometry, the positions of the sources are unknown and $\partial\mathbb{D}$ can be very irregular. In that case, the best one can do is to replace the operation $n_i\partial_i$ by a factor $-jk$, which leads to

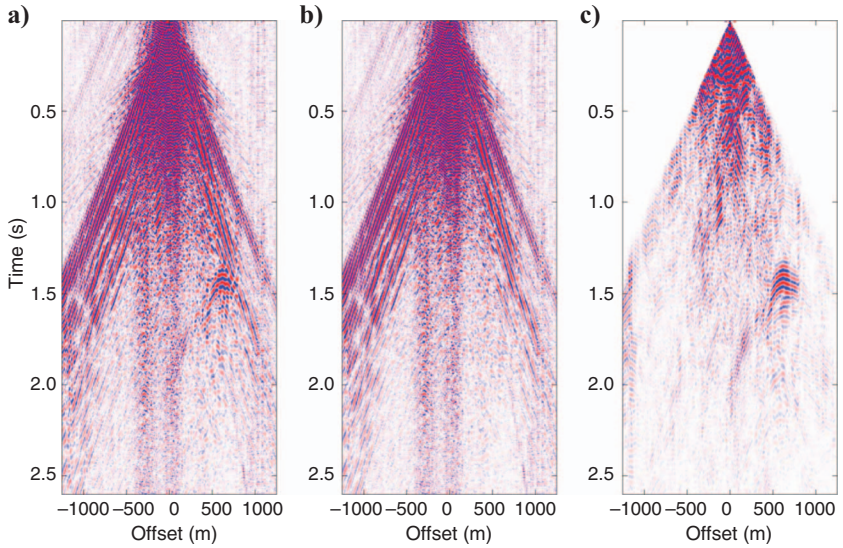

Figure 5. Example of interferometric ground-roll removal applied to shot records while preserving the direct ground roll (Halliday et al., 2010a). (a) Raw data. (b) Results of interferometric scattered ground roll removal. (c) The subtracted scattered ground roll.

$$\hat{G}(\mathbf{x}_B,\mathbf{x}_A,\omega) + \hat{G}^*(\mathbf{x}_B,\mathbf{x}_A,\omega) \approx \frac{2}{\rho c}\oint_{\partial\mathbb{D}} \hat{G}(\mathbf{x}_B,\mathbf{x},\omega)\hat{G}^*(\mathbf{x}_A,\mathbf{x},\omega)\mathrm{d}^2\mathbf{x}. \quad (16)$$

This approximation is accurate when $\partial\mathbb{D}$ is a sphere with large radius so that all rays are approximately normal to $\partial\mathbb{D}$ (i.e., $\alpha \approx 0$). For arbitrary surfaces, equation 16 involves an amplitude error. Moreover, spurious events may occur due to incomplete cancellation of contributions from different stationary points. However, because the approximation does not affect the phase, equation 16 is usually considered acceptable for seismic interferometry. Transforming both sides of equation 16 back to the time domain yields

$$G(\mathbf{x}_B,\mathbf{x}_A,t) + G(\mathbf{x}_B,\mathbf{x}_A,-t) \approx \frac{2}{\rho c}\oint_{\partial\mathbb{D}} G(\mathbf{x}_B,\mathbf{x},t) * G(\mathbf{x}_A,\mathbf{x},-t)\mathrm{d}^2\mathbf{x}, \quad (17)$$

which is equal to equation 4, i.e., the expression obtained by Derode et al. (2003a, b) with proportionality factor $2/\rho c$.

Of course, there are situations for which the derivation presented above does not apply. For example, when $\partial\mathbb{D}$ is enclosing the water layer for marine seismology applications, the assumption that the medium is homogeneous outside $\partial\mathbb{D}$ breaks down and the derivatives of the Green's functions must be obtained in another way. Ramírez and Weglein (2009) discuss a correlation-based processing scheme for ocean-bottom data, based on a variant of equation 11, in which the time-reversed Green's function and its derivative are taken as analytic direct-wave solutions in the water layer. In the following, we restrict the application of equations 15–17 to situations for which they were derived.

The practical application of equations 11 and 15–17 requires discretization of the integrals. The accuracy depends on the regularity of the distribution of the sources along $\partial\mathbb{D}$ (van Manen et al., 2005; Fan and Snieder, 2009; Yao and van der Hilst, 2009). A bias can be introduced in Green's function estimates when amplitudes of energy have directional variations. Curtis and Halliday (2010a) present an algorithm to remove this bias. In the "Interferometry by multidimensional deconvolution" section, we present another effective way to compensate for illumination irregularities.

Equations 11 and 15–17 have been used for interferometric wavefield modeling (van Manen et al., 2005) as well as for the derivation of passive and controlled-source seismic interferometry. For passive interferometry, the configuration is chosen similarly to Figure 4, in which a part of the closed boundary $\partial\mathbb{D}$ is a free surface at which no sources are required; thus, the closed boundary integral reduces to an integral over the remaining part $\partial\mathbb{D}_1$. When the sources on $\partial\mathbb{D}_1$ are noise sources, the responses at $\mathbf{x}_A$ and $\mathbf{x}_B$ are given by $u(\mathbf{x}_A,t) = \int_{\partial\mathbb{D}_1} G(\mathbf{x}_A,\mathbf{x},t) * N(\mathbf{x},t)\mathrm{d}^2\mathbf{x}$ and $u(\mathbf{x}_B,t) = \int_{\partial\mathbb{D}_1} G(\mathbf{x}_B,\mathbf{x}',t) * N(\mathbf{x}',t)\mathrm{d}^2\mathbf{x}'$, respectively. Assuming the noise sources are mutually uncorrelated, according to $\langle N(\mathbf{x}',t) * N(\mathbf{x},-t)\rangle = \delta(\mathbf{x}-\mathbf{x}')S_N(t)$ for $\mathbf{x}$ and $\mathbf{x}'$ on $\partial\mathbb{D}_1$, the crosscorrelation of the responses at $\mathbf{x}_A$ and $\mathbf{x}_B$ gives

$$\langle u(\mathbf{x}_B,t) * u(\mathbf{x}_A,-t)\rangle = \int_{\partial\mathbb{D}_1} G(\mathbf{x}_B,\mathbf{x},t) * G(\mathbf{x}_A,\mathbf{x},-t) * S_N(t)\mathrm{d}^2\mathbf{x}. \quad (18)$$

Combining this with equation 17, we obtain

$$\{G(\mathbf{x}_B,\mathbf{x}_A,t) + G(\mathbf{x}_B,\mathbf{x}_A,-t)\} * S_N(t) \approx \frac{2}{\rho c}\langle u(\mathbf{x}_B,t) * u(\mathbf{x}_A,-t)\rangle. \quad (19)$$

Representations 17 and 19 can be seen as alternatives for equations 13 and 14 in Part 1. The main difference is that, in the present derivation, we did not need to neglect evanescent waves; the receiver positions $\mathbf{x}_A$ and $\mathbf{x}_B$ can be anywhere in $\mathbb{D}$ (instead of at the free surface).

Schuster (2009) uses equations 11 and 15–17 for the theoretical justification of controlled-source interferometry in any of the configurations in Figure 11 of Part 1. Korneev and Bakulin (2006) use the same equations to explain the theory of the virtual-source method illustrated in Figure 2 of the current paper. In none of these configurations do the sources form a closed boundary around the receivers at $\mathbf{x}_A$ and $\mathbf{x}_B$, as prescribed by the theory, so the closed boundary integral is by necessity replaced by an open boundary integral. Assuming the medium is sufficiently inhomogeneous such that all energy is scattered back to the receivers, one-sided illumination suffices (Wapenaar, 2006a). However, in many practical situations, this condition is not fulfilled; so the open boundary integral introduces artifacts, often denoted as spurious multiples (Snieder et al., 2006b).

A partial solution, implemented by Bakulin and Calvert (2006), is to apply a time window to $G(\mathbf{x}_A,\mathbf{x},t)$ in equation 17 (or $u(\mathbf{x}_A,\mathbf{x}_S^{(i)},t)$ in equation 1) with the aim of selecting direct waves only. The artifacts can be further suppressed by applying up/down decomposition to both Green's functions in the right-hand side of equation 17 (Mehta et al., 2007a; van der Neut and Wapenaar, 2009). Note that in the latter two cases, the direct-wave part of $G(\mathbf{x}_A,\mathbf{x},t)$ (or $u(\mathbf{x}_A,\mathbf{x}_S^{(i)},t)$ in equation 1) propagates only through the overburden. This implies that the condition of having a lossless medium only applies to the overburden; hence, the medium below the receivers in Figure 2 may be attenuating. This is shown more rigorously by Slob and Wapenaar (2007a) and Vasconcelos et al. (2009). An even more effective suppression of artifacts related to one-sided illumination is discussed in the "Interferometry by multidimensional deconvolution" section.

RECENT AND NEW ADVANCES

The previous discussion covers the current state of seismic interferometry. Here, we briefly indicate some recent and new advances.

Media with losses

Until now, we generally assumed that the medium under investigation is lossless and nonmoving, which is equivalent to assuming that the underlying wave equation is invariant for time reversal. Moreover, in all cases, the Green's functions obey source-receiver reciprocity. In a medium with losses, the wave equation is no longer invariant for time reversal; but as long as the medium is not moving, source-receiver reciprocity still holds. When the losses are not too high, the methods discussed above yield a Green's function with correct traveltimes and approximate amplitudes (Roux et al., 2005; Slob and Wapenaar, 2007b).

Snieder (2007) shows that when the losses are significant, a volume integral $-2\omega\int_{\mathbb{D}}\hat{\kappa}_i(\mathbf{x},\omega)\hat{G}(\mathbf{x}_B,\mathbf{x},\omega)\hat{G}^*(\mathbf{x}_A,\mathbf{x},\omega)\mathrm{d}^3\mathbf{x}$ (where $\hat{\kappa}_i(\mathbf{x},\omega)$ denotes the imaginary part of the compressibility) should be added to the right-hand side of any of equations 11, 15 or 16 (actually, the negative sign in front of the integral is absent in Snieder's analysis because he uses another convention for the Fourier transform). Thus, in addition to the requirement of having sources at the

boundary $\partial\mathbb{D}$ (as in Figures 3c and 4), sources are required throughout the domain $\mathbb{D}$. When these sources are uncorrelated noise sources, the final expression for Green's function retrieval again has a similar form as equation 19. This volume integral approach to Green's function retrieval is not restricted to acoustic waves in lossy media but also applies to electromagnetic waves in conductive media (Slob and Wapenaar, 2007a) as well as to pure diffusion phenomena (Snieder, 2006).

In most practical situations, sources are not available throughout a volume. Interferometry by crossconvolution (Slob et al., 2007a; Halliday and Curtis, 2009b) is another approach that accounts for losses. Draganov et al. (2010) compensate for losses with an inverse attenuation filter. By doing this adaptively (aiming to minimize artifacts), they estimate the attenuation parameters. The methodology discussed in the "Interferometry by multidimensional deconvolution" section also accounts very effectively for losses.

Nonreciprocal media

In a moving medium (with or without losses), time-reversal invariance and source-receiver reciprocity break down. It has been shown that with some modifications, time-reversed acoustic focusing (as in Figure 1) can still work in a moving medium (Dowling, 1993; Roux et al., 2004). Using reciprocity theory, it follows that Green's function retrieval by crosscorrelation is also possible in a moving medium (Godin, 2006; Wapenaar, 2006b). The required modification to the Green's function representation is surprisingly simple: The time-reversed Green's function $G(\mathbf{x}_B,\mathbf{x}_A,-t)$ on the left-hand side of equations 17 and 19 should be replaced by $G(\mathbf{x}_A,\mathbf{x}_B,-t)$, assuming all Green's functions appearing in the representation are defined in the moving medium. Hence, in nonreciprocal media, the retrieved function $G(\mathbf{x}_B,\mathbf{x}_A,t)+G(\mathbf{x}_A,\mathbf{x}_B,-t)$ is no longer time symmetric (see Figure 6 for a 1D illustration). Interferometry in moving media has potential applications in solar seismology and in infrasound (Evers and Siegmund, 2009; Haney, 2009).

With similar simple modifications, global-scale interferometry accounts for the Coriolis force of a rotating earth (Ruigrok et al., 2008) and electromagnetic interferometry accounts for nonreciprocal effects in bianisotropic media (Slob and Wapenaar, 2009). A moving conductive medium in the presence of a static magnetic field is an example of a bianisotropic medium. Electromagnetic interferometry in bianisotropic media may find applications in controlled-source electromagnetic (CSEM) acquisition with receivers in the air in areas with strong tidal currents.

Unified formulations

The wave equation for a medium with losses can be seen as a special case of the more general differential equation,

$$\left[\sum_{n=1}^{N} a_n(\mathbf{x},t)*\frac{\partial^n}{\partial t^n}-H(\mathbf{x},t)*\right]u(\mathbf{x},t)=s(\mathbf{x},t), \quad (20)$$

where $a_n(\mathbf{x},t)$ are medium parameters, $H(\mathbf{x},t)$ is a spatial differential operator, and $s(\mathbf{x},t)$ is a source function. Snieder et al. (2007) derive unified Green's function representations for fields obeying this differential equation, assuming $H(\mathbf{x},t)$ is either symmetric or antisymmetric. These representations, consisting of a boundary and a volume integral, capture interferometry for acoustic wave propagation (with or without losses), diffusion, advection, bending waves in mechanical structures, and quantum mechanical scattering problems. Weaver (2008) provides an alternative derivation based on Ward identities. A recent extension (Snieder et al., 2010) also accounts for potential fields (for which all $a_n=0$ and H is independent of time in equation 20).

Similarly, for a matrix-vector differential equation of the form

$$\left[\mathbf{A}(\mathbf{x},t)*\frac{D}{Dt}+\mathbf{D}_{\mathbf{x}}+\mathbf{B}(\mathbf{x},t)*\right]\mathbf{u}(\mathbf{x},t)=\mathbf{s}(\mathbf{x},t), \quad (21)$$

where $\mathbf{A}$ and $\mathbf{B}$ are medium-parameter matrices, D/Dt the material time derivative, and $\mathbf{D}_{\mathbf{x}}$ a spatial differential operator matrix, a unified Green's matrix representation has been derived (Wapenaar et al., 2006). This representation, again consisting of a boundary and a volume integral, captures interferometry for acoustic, elastodynamic, electromagnetic, poroelastic, piezoelectric, and electroseismic wave propagation as well as for diffusion and flow. For the situation of uncorrelated noise sources distributed along a boundary (for lossless media) or throughout a volume (for media with losses), the unified Green's matrix representation is given by

$$\{\mathbf{G}(\mathbf{x}_B,\mathbf{x}_A,t)+\mathbf{G}^t(\mathbf{x}_A,\mathbf{x}_B,-t)\}*S_N(t)\approx\langle\mathbf{u}(\mathbf{x}_B,t)*\mathbf{u}^t(\mathbf{x}_A,-t)\rangle \quad (22)$$

(superscript t denotes transposition), where $\mathbf{u}(\mathbf{x}_A,t)$ and $\mathbf{u}(\mathbf{x}_B,t)$ are the noise responses at $\mathbf{x}_A$ and $\mathbf{x}_B$, respectively. In subscript notation, this becomes

$$\{G_{qp}(\mathbf{x}_B,\mathbf{x}_A,t)+G_{pq}(\mathbf{x}_A,\mathbf{x}_B,-t)\}*S_N(t)\approx\langle u_q(\mathbf{x}_B,t)*u_p(\mathbf{x}_A,-t)\rangle. \quad (23)$$

Note the resemblance to equation 10 for elastodynamic Green's function retrieval. For electroseismic waves, $\mathbf{u}^t=(\mathbf{E}^t,\mathbf{H}^t,\{\mathbf{v}^s\}^t,-\boldsymbol{\tau}_1^t,-\boldsymbol{\tau}_2^t,\mathbf{w}^t,p^f)$, where $\mathbf{E}$ and $\mathbf{H}$ are the electric and magnetic field vectors, $\mathbf{v}^s$ the particle velocity of the solid phase, $\boldsymbol{\tau}_i$ the traction, $\mathbf{w}$ the filtration velocity of the fluid through the pores, and p^f the pressure of the fluid phase. Accordingly, for example, the (9,1) element of $\mathbf{G}(\mathbf{x}_B,\mathbf{x}_A,t)$, i.e., $G_{9,1}(\mathbf{x}_B,\mathbf{x}_A,t)$, is the vertical particle velocity of the solid phase at $\mathbf{x}_B$ from an impulsive horizontal electric current source at $\mathbf{x}_A$. According to equations 22 and 23, it is retrieved by crosscorrelating the ninth element of $\mathbf{u}(\mathbf{x}_B,t)$, i.e., the vertical velocity noise

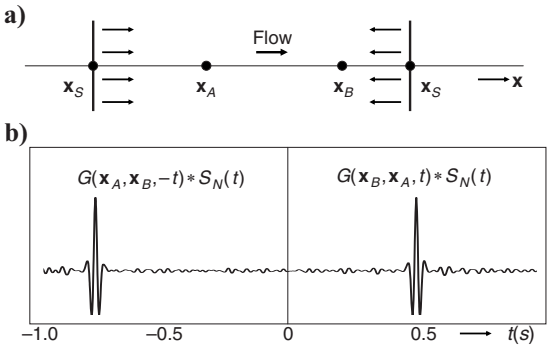

Figure 6. A 1D example of direct-wave interferometry in a moving medium. (a) Rightward- and leftward-propagating noise signals in a rightward-flowing medium. (b) Crosscorrelation of the responses at x_A and x_B. The causal part stems from the rightward-propagating wave and is interpreted as the Green's function propagating "downwind" from x_A to x_B. The acausal part stems from the leftward-propagating wave and is interpreted as the time-reversed Green's function propagating "upwind" from x_B to x_A.

field at $\mathbf{x}_B$ with the first element of $\mathbf{u}(\mathbf{x}_A,t)$ being the horizontal electric noise field at $\mathbf{x}_A$ (Figure 7). For a further discussion on electroseismic interferometry, including numerical examples, see de Ridder et al. (2009).

Relation with the generalized optical theorem

It has recently been recognized (Snieder et al., 2008; Halliday and Curtis, 2009a) that the frequency-domain Green's function representation for seismic interferometry resembles the generalized optical theorem (Heisenberg, 1943; Glauber and Schomaker, 1953; Newton, 1976; Marston, 2001), given by

$$\frac{-1}{2j}\{f(\mathbf{k}_A,\mathbf{k}_B) - f^*(\mathbf{k}_B,\mathbf{k}_A)\} = \frac{k}{4\pi}\oint f(\mathbf{k},\mathbf{k}_B)f^*(\mathbf{k},\mathbf{k}_A)\mathrm{d}\Omega, \tag{24}$$

where $f(\mathbf{k}_A,\mathbf{k}_B)$ is the far-field angle-dependent scattering amplitude of a finite scatterer (Figure 8), including all linear and nonlinear interactions of the wavefield with the scatterer.

The optical theorem has a form similar to interferometry representation 16 for acoustic waves. The analysis of this resemblance has led to new insights in interferometry as well as in scattering theorems. Snieder et al. (2008) use the generalized optical theorem to explain the cancellation of specific spurious arrivals in Green's function extraction. Halliday and Curtis (2009a) show that the generalized optical theorem can be derived from the interferometric Green's function representation and use this to derive an optical theorem for surface waves in layered elastic media. Snieder et al. (2009b) discuss how the scattering amplitude can be derived from field fluctuations. In other related work, Halliday and Curtis (2009b) and Wapenaar et al. (2010) show that the Born approximation is an insufficient model to explain all aspects of seismic interferometry, even for the situation of a single point scatterer, and use this insight to derive improved models for the scattering amplitude of a point scatterer.

Virtual receivers, reflectors, and imaging

Until now, we have discussed seismic interferometry as a method that retrieves the response of a virtual source by crosscorrelating responses at two receivers. Using reciprocity, it is also possible to create a virtual receiver by crosscorrelating the responses of two sources. Curtis et al. (2009) use this principle to turn earthquake sources into virtual seismometers with which real seismograms can be recorded, located noninvasively deep within the earth's subsurface. They argue that this methodology has the potential to improve the resolution of imaging the earth's interior by earthquake seismology. An earthquake source acts like a double couple; so by reciprocity, the virtual receiver acts like a strainmeter, a device that is not easily implemented by a physical instrument. In a similar way, microseismic sources near a reservoir could be turned into virtual receivers to improve the resolution of reservoir imaging (Figure 9). Note that imaging using virtual receivers requires knowledge of the position of the sources, but recording seismograms on the virtual seismometers does not.

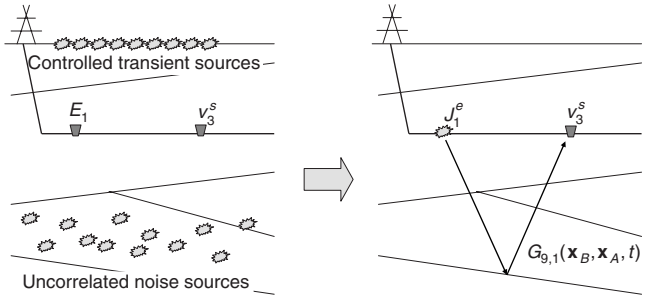

Figure 7. Principle of electroseismic interferometry for controlled transient sources at the surface or uncorrelated noise sources in the subsurface. In this example, the vertical component of the particle velocity of the solid phase is crosscorrelated with the horizontal component of the electric field, yielding the electroseismic response of a horizontal electric current source observed by a vertical geophone.

Another variant is the virtual reflector method (Poletto and Farina, 2008; Poletto and Wapenaar, 2009). This method creates new seismic signals by processing real seismic responses of impulsive or transient sources. Under proper recording coverage conditions, this technique obtains seismograms as if there were an ideal reflector at the position of the receivers (or sources). The algorithm consists of convolution of the recorded traces, followed by integration of the crossconvolved signals along the receivers (or sources). Similar to other interferometry methods, the virtual reflector method does not require information on the propagation velocity of the medium. Poletto and Farina (2010) illustrate the method with synthetic marine and real borehole data.

Curtis (2009), Schuster (2009, chapter 8), and Curtis and Halliday (2010b) discuss source-receiver interferometry. This method combines the virtual-source and the virtual-receiver methodologies and thus involves a double integration over sources and receivers. It creates the response of a virtual source observed by a virtual receiver. This method is related to prestack redatuming (Berryhill, 1984), in which sources and receivers are repositioned from the acquisition surface to a new datum plane in the subsurface, using one-way wavefield extrapolation operators based on a macromodel. In source-receiver interferometry, the operators are replaced by measured responses — for example, in VSPs. Hence, source-receiver interferometry can be seen as the data-driven variant of prestack redatuming.

Note, however, that in general the measured responses used in source-receiver interferometry are full wavefields rather than one-way operators. Therefore, the application of source-receiver interferometry is not restricted to data-driven prestack redatuming, but it can be used for other applications as well. For example, Halliday et al. (2010b) show that the elastodynamic version of source-receiver interferometry can be seen as a generalization of a method that turns

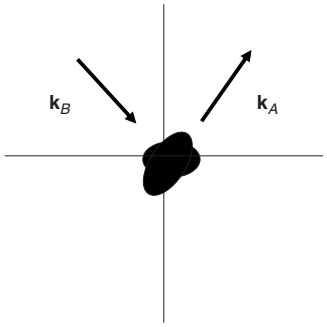

Figure 8. The generalized optical theorem for the angle-dependent scattering amplitude $f(\mathbf{k}_A,\mathbf{k}_B)$ (Heisenberg, 1943) has a similar form as the Green's function representation for seismic interferometry.

PP and PS data into SS data, previously proposed by Grechka and Tsvankin (2002) and Grechka and Dewangan (2003). In a similar fashion, the internal multiple prediction method of Jakubowicz (1998) can be derived as a special case of source-receiver interferometry. Also, the surface-wave-removal methods of Dong et al. (2006), Curtis et al. (2006), and Halliday et al. (2007, 2010a) require physically recorded and interferometrically constructed Green's function estimates between the locations of an active source and active receiver. Previously, the interferometric estimate was obtained by having to place a receiver beside every source and turning the former into a virtual source (or vice versa, using virtual-receiver interferometry). However, by using source-receiver interferometry, this becomes unnecessary because the interferometric wavefield estimate can be made between real source and real receiver directly (Curtis and Halliday, 2010b).

Similar double integrals appear in the acoustic inverse scattering imaging formulation of Oristaglio (1989). Halliday and Curtis (2010) derive explicitly a generalized version of Oristaglio's formulation from a version of source-receiver interferometry for a medium with scattering perturbations. The derivation was possible because this form of interferometry is the first to combine active sources and receivers, similar to geometries used for imaging.

Time-lapse seismic interferometry

As a consequence of the stability of time-reversed acoustics, seismic interferometry has large potential for time-lapse methods. We have indicated the use of passive interferometry for monitoring changes in volcanic interiors (Sens-Schönfelder and Wegler, 2006; Brenguier et al., 2008b). Using the same principles, Brenguier et al. (2008a) monitor postseismic relaxation along the San Andreas fault at Parkfield, California, U.S.A., and Ohmi et al. (2008) monitor temporal variations of the crustal structure in the source region of the 2007 Noto Hanto earhquake in central Japan. Kraeva et al. (2009) show a relation between seasonal variations of ambient noise crosscorrelations and remote microseismic activity related to ocean storms, and Haney (2009) reports on time-dependent effects in correlations of infrasound that arise from time-varying temperature fields and temperature inversion layers in the atmosphere. The interpretation in all these methods is based on measuring the time shift in either the direct wave or the coda wave of the Green's functions retrieved by interferometry. These time shifts give information about the average velocity change between the receivers, which can be further regionalized by tomographic inversion (Brenguier et al., 2008b).

In the field of controlled-source interferometry, Bakulin et al. (2007) and Mehta et al. (2008) discuss the potential of the virtual-source method for time-lapse reservoir monitoring. They exploit the fact that virtual-source data are obtained from permanent downhole or ocean-bottom-cable receivers and hence have a high degree of repeatability. Because virtual-source data represent reflection responses, local time-lapse changes in these data can be reliably attributed to local changes in the reservoir.

To better quantify the time-lapse changes in the data obtained by seismic interferometry, the interferometric Green's function representation (equation 11) has been modified to account for time-lapse changes according to

$$\begin{aligned}\hat{G}(\mathbf{x}_B,\mathbf{x}_A,\omega) + \hat{\bar{G}}^*(\mathbf{x}_B,\mathbf{x}_A,\omega)\\ = -\oint_{\partial\mathbb{D}} \frac{1}{j\omega\rho(\mathbf{x})}((\partial_i\hat{G}(\mathbf{x}_B,\mathbf{x},\omega))\hat{\bar{G}}^*(\mathbf{x}_A,\mathbf{x},\omega)\\ - \hat{G}(\mathbf{x}_B,\mathbf{x},\omega)\partial_i\hat{\bar{G}}^*(\mathbf{x}_A,\mathbf{x},\omega))n_i\mathrm{d}^2\mathbf{x}\\ + j\omega\int_{\mathbb{D}}\Delta\hat{\kappa}(\mathbf{x},\omega)\hat{G}(\mathbf{x}_B,\mathbf{x},\omega)\hat{\bar{G}}^*(\mathbf{x}_A,\mathbf{x},\omega)\mathrm{d}^3\mathbf{x}, \qquad (25)\end{aligned}$$

with $\Delta\hat{\kappa}(\mathbf{x},\omega) = \hat{\kappa}(\mathbf{x},\omega) - \hat{\bar{\kappa}}^*(\mathbf{x},\omega)$ (Vasconcelos and Snieder, 2008a; Douma, 2009; Vasconcelos et al., 2009). Here, the quantities with/without a bar refer to the reference/monitor state (for simplicity, we assume that time-lapse changes occur only in the compressibility). The equivalent theory for source-receiver interferometry is given in Halliday and Curtis (2010). Equation 25 and its generalization for other wave types (Wapenaar, 2007) provides a basis for deriving local time-lapse changes of the medium parameters from interferometric time-lapse data. This is the subject of ongoing research.

Interferometry by deconvolution and crosscoherence

In the previous treatment of interferometry, we focused on Green's function extraction by crosscorrelation. Time reversal corresponds to complex conjugation in the frequency domain, so the crosscorrelation is, in the frequency domain, given by

$$\hat{C}(\mathbf{x}_B,\mathbf{x}_A,\omega) = \hat{u}(\mathbf{x}_B,\omega)\hat{u}^*(\mathbf{x}_A,\omega). \qquad (26)$$

According to expression 19, the crosscorrelation does not just give the superposition of the Green's function and its time-reversed counterpart because the left-hand side of that expression is convolved with the autocorrelation of the noise that excites the field fluctuations. This means that equation 26 gives the product of the Green's function and the power spectrum $\hat{S}_N(\omega)$ of the noise. The power spectrum thus leaves an imprint on the extracted Green's function unless it is properly accounted for. This imprint can be eliminated by using deconvolution instead of crosscorrelation. In the frequency domain, deconvolution corresponds to spectral division; hence, the deconvolution approach consists of replacing expression 26 by

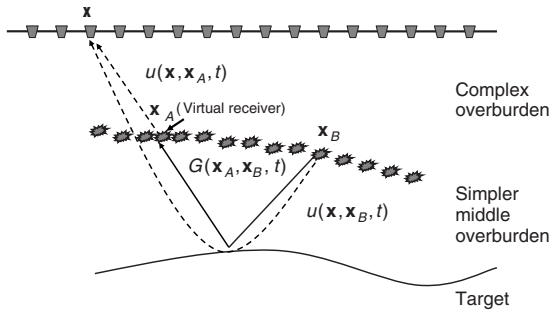

Figure 9. Using reciprocity, Bakulin and Calvert's virtual-source method (Figure 2) can be reformulated into a virtual receiver method. Receivers at the surface record the direct and the reflection responses of microseismic sources above a deeper target. Crosscorrelation and summing over receiver locations gives the reflection response at a virtual receiver at the position of a microseismic source, free of overburden distortions.

$$\hat{D}(\mathbf{x}_B,\mathbf{x}_A,\omega) = \frac{\hat{u}(\mathbf{x}_B,\omega)}{\hat{u}(\mathbf{x}_A,\omega)}. \quad (27)$$

When $\hat{u}(\mathbf{x}_A,\omega)$ is small, this spectral division is unstable. In practice, one needs to regularize the deconvolution. The simplest way to do this is to use the following water-level regularization:

$$\hat{D}(\mathbf{x}_B,\mathbf{x}_A,\omega) = \frac{\hat{u}(\mathbf{x}_B,\omega)\hat{u}^*(\mathbf{x}_A,\omega)}{|\hat{u}(\mathbf{x}_A,\omega)|^2 + \varepsilon^2}, \quad (28)$$

where ε^2 is a stabilization parameter. When $\varepsilon^2 = 0$, expression 28 reduces to equation 27; for $\varepsilon^2 \gg |\hat{u}(\mathbf{x}_A,\omega)|^2$, equation 28 corresponds to a scaled version of the correlation defined in expression 26.

A significant difference between crosscorrelation and deconvolution is that crosscorrelation gives the Green's function but deconvolution does not. This raises the question, what wave state is retrieved by deconvolving field measurements recorded at different points? There is a simple proof that the wave states obtained by crosscorrelation, deconvolution, and regularized deconvolution all satisfy the same equation as the real system does (Snieder et al., 2006a). Let us denote the field equation of the system by

$$\hat{L}(\mathbf{x},\omega)\hat{u}(\mathbf{x},\omega) = 0. \quad (29)$$

For the acoustic wave equation in a constant-density medium, for example, the operator $\hat{L}$ is given by $\hat{L}(\mathbf{x},\omega) = \nabla^2 + \omega^2/c^2(\mathbf{x})$. The right-hand side of expression 29 equals zero, so this expression holds for source-free regions, which is the case at the receivers. Applying $\hat{L}$ to equation 27 with $\mathbf{x}_B$ replaced by $\mathbf{x}$ gives

$$\hat{L}(\mathbf{x},\omega)\hat{D}(\mathbf{x},\mathbf{x}_A,\omega) = \hat{L}(\mathbf{x},\omega)\left(\frac{\hat{u}(\mathbf{x},\omega)}{\hat{u}(\mathbf{x}_A,\omega)}\right)$$

$$= \frac{1}{\hat{u}(\mathbf{x}_A,\omega)}\hat{L}(\mathbf{x},\omega)\hat{u}(\mathbf{x},\omega) = 0, \quad (30)$$

where in the second identity we used that $\hat{L}(\mathbf{x},\omega)$ acts on the $\mathbf{x}$-coordinates only and where the field equation 29 is used in the last identity. The same reasoning applies to the correlation of expression 26 and the regularized deconvolution in expression 28. All of these procedures thus produce a wave state that satisfies the same wave equation as the original system does. For the correlation, this wave state is the Green's function; but for the deconvolution, a different wave state is obtained.

To understand which wave state is extracted by deconvolution, we note that

$$\hat{D}(\mathbf{x}_A,\mathbf{x}_A,\omega) = \frac{\hat{u}(\mathbf{x}_A,\omega)}{\hat{u}(\mathbf{x}_A,\omega)} = 1. \quad (31)$$

This corresponds, in the time domain, to

$$D(\mathbf{x}_A,\mathbf{x}_A,t) = \delta(t). \quad (32)$$

Deconvolution thus gives a wave state that, for $t \neq 0$, vanishes at the virtual-source location $\mathbf{x}_A$. This means that the wavefield vanishes at that location, and hence, the phrase "clamped boundary condition" has been used (Vasconcelos and Snieder, 2008a). Deconvolution thus gives a wave state where the field vanishes at one point in space. This wave state is, in general, not equal to the Green's function.

Despite this strange boundary condition, interferometry by deconvolution has a distinct advantage for attenuating media. Consider the example of Figure 1a of Part 1 of this tutorial where a plane wave propagates along a line from a source at x_S to receivers at x_A and x_B, respectively. For a homogeneous attenuating medium, the field recorded at x_A equals $\hat{u}(x_A,\omega) = \hat{G}(x_A,x_S,\omega)\hat{N}(\omega) = \exp(-\gamma(x_A - x_S))\exp(-jk(x_A - x_S))\hat{N}(\omega)$, where γ is an attenuation coefficient and $\hat{N}(\omega)$ is the source spectrum. A similar expression holds for the field at x_B. The correlation of the fields recorded at x_A and x_B is given by

$$\hat{C}(x_B,x_A,\omega) = e^{-\gamma(x_A + x_B - 2x_S)}e^{-jk(x_B - x_A)}\hat{S}_N(\omega), \quad (33)$$

with $\hat{S}_N(\omega) = |\hat{N}(\omega)|^2$. This field has the same phase as the field that propagates from x_A to x_B, but the attenuation is incorrect because it depends on the source location x_S, which is, of course, not related to the field that propagates between x_A and x_B. In contrast, the deconvolution of the recorded fields satisfies

$$\hat{D}(x_B,x_A,\omega) = e^{-\gamma(x_B - x_A)}e^{-jk(x_B - x_A)} = \hat{G}(x_B,x_A,\omega), \quad (34)$$

which does correctly account for the phase and the amplitude and which does not depend on $\hat{N}(\omega)$. This property of the deconvolution approach for 1D systems has been used to extract the velocity and attenuation in the near surface (Trampert et al., 1993; Mehta et al., 2007b) and to determine the structural response of buildings from incoherent ground motion (Snieder and Şafak, 2006; Thompson and Snieder, 2006; Kohler et al., 2007). The deconvolution method has even been used to detect changes in the near-surface shear-wave velocity during shaking caused by an earthquake (Sawazaki et al., 2009).

The application of deconvolution interferometry changes when one can separate the wavefield into an unperturbed wave u_0 and a perturbation u_S (Vasconcelos and Snieder, 2008b). Such a separation can be achieved by time gating when impulsive shots are used (Bakulin et al., 2007; Mehta et al., 2007a), by using array methods, or by using four-component data. In this case, one can define a new deconvolution,

$$\hat{D}'(\mathbf{x}_B,\mathbf{x}_A,\omega) = \frac{\hat{u}_S(\mathbf{x}_B,\omega)}{\hat{u}_0(\mathbf{x}_A,\omega)}, \quad (35)$$

which gives an estimate of the perturbed Green's function $\hat{G}_S$. This modified deconvolution method has been used to illuminate the San Andreas fault from the side using drill-bit noise (Figure 10) and for subsalt imaging from below using internal multiples (Vasconcelos et al., 2008). A comparison of crosscorrelation, deconvolution, and multidimensional deconvolution (presented in the next section) is given by Snieder et al. (2009a).

A method related to deconvolution is crosscoherence, defined as

$$\hat{H}(\mathbf{x}_B,\mathbf{x}_A,\omega) = \frac{\hat{u}(\mathbf{x}_B,\omega)}{|\hat{u}(\mathbf{x}_B,\omega)|}\frac{\hat{u}^*(\mathbf{x}_A,\omega)}{|\hat{u}(\mathbf{x}_A,\omega)|}. \quad (36)$$

The crosscoherence can be seen as a spectrally normalized crosscorrelation or as a variant of deconvolution that is symmetric in $\hat{u}(\mathbf{x}_A,\omega)$ and $\hat{u}(\mathbf{x}_B,\omega)$. This method of combining data is proposed by Aki in his seminal papers on retrieving surface waves from microtremors (1957, 1965). It has been used extensively in engineering (Bendat and Piersol, 2000) in the extraction of response functions and is commonly used to determine shallow shear velocity from ground vibrations, e.g., Chávez-García and Luzón (2005). Note that the reason-

ing leading to equation 30 is not applicable to the crosscoherence because of the presence of the normalized spectrum in the denominator of expression 36. Hence, the crosscoherence does not necessarily lead to a wave state that satisfies the same equation as the real system does.

Interferometry by multidimensional deconvolution

Interferometry by multidimensional deconvolution (MDD) is the natural extension of interferometry by deconvolution to two or three dimensions. It has been proposed for controlled-source data (Schuster and Zhou, 2006; Wapenaar et al., 2008a) as well as for passive data (Wapenaar et al., 2008b). Here, we discuss the principle for controlled-source data and briefly indicate the modifications for noise data.

Consider again Figure 2, which we initially used to introduce the virtual-source method of Bakulin and Calvert (2004). We express the upgoing wavefield at $\mathbf{x}_B$ as

$$u^-(\mathbf{x}_B,\mathbf{x}_S^{(i)},t) = \int G(\mathbf{x}_B,\mathbf{x}_A,t)*u^+(\mathbf{x}_A,\mathbf{x}_S^{(i)},t)\mathrm{d}\mathbf{x}_A, \quad (37)$$

where the plus and minus superscripts refer to downgoing and upgoing waves, respectively. Note that the integration takes place along the receivers at $\mathbf{x}_A$ in the borehole. This convolutional data representation is valid in media with or without losses. However, unlike equation 1, which is an explicit but approximate expression for the Green's function $G(\mathbf{x}_B,\mathbf{x}_A,t)$ (convolved with the autocorrelation $S_s(t)$ of the source wavelet), equation 37 is an implicit but exact expression for $G(\mathbf{x}_B,\mathbf{x}_A,t)$ (with $G(\mathbf{x}_B,\mathbf{x}_A,t)$ being the reflection response of the medium below the receiver level with a homogeneous half-space above it [Wapenaar, Slob, et al., 2008]). Equation 37 can be solved by MDD, assuming responses are available for many source positions $\mathbf{x}_S^{(i)}$. In that case, equation 37 holds for each source separately. In the frequency domain, the resulting set of simultaneous equations can be represented in matrix notation (Berkhout, 1982) according to

$$\hat{\mathbf{U}}^- = \hat{\mathbf{G}}\hat{\mathbf{U}}^+, \quad (38)$$

where the (j,i) element of $\hat{\mathbf{U}}^+$ is given by $\hat{u}^+(\mathbf{x}_A^{(j)},\mathbf{x}_S^{(i)},\omega)$, etc. Equation 38 can be solved for $\hat{\mathbf{G}}$, e.g., via weighted least-squares inversion (Menke, 1989), according to

$$\hat{\mathbf{G}} = \hat{\mathbf{U}}^-\mathbf{W}\{\hat{\mathbf{U}}^+\}^\dagger(\hat{\mathbf{U}}^+\mathbf{W}\{\hat{\mathbf{U}}^+\}^\dagger + \varepsilon^2\mathbf{I})^{-1}, \quad (39)$$

where the dagger denotes transposition and complex conjugation, $\mathbf{W}$ is a diagonal weighting matrix, $\mathbf{I}$ is the identity matrix, and ε^2 is a stabilization parameter. Equation 39 is the multidimensional extension of equation 28. Applying this equation for each frequency component and transforming the result to the time domain accomplishes interferometry by MDD.

To get more insight into equation 37 and its solution by MDD, we convolve both sides with the time-reversed downgoing wavefield $u^+(\mathbf{x}'_A,\mathbf{x}_S^{(i)},-t)$ and sum over the source positions $\mathbf{x}_S^{(i)}$ (van der Neut et al., 2010). This gives

$$C(\mathbf{x}_B,\mathbf{x}'_A,t) = \int G(\mathbf{x}_B,\mathbf{x}_A,t)*\Gamma(\mathbf{x}_A,\mathbf{x}'_A,t)\mathrm{d}\mathbf{x}_A, \quad (40)$$

with

$$C(\mathbf{x}_B,\mathbf{x}'_A,t) = \sum_i u^-(\mathbf{x}_B,\mathbf{x}_S^{(i)},t)*u^+(\mathbf{x}'_A,\mathbf{x}_S^{(i)},-t) \quad (41)$$

and

$$\Gamma(\mathbf{x}_A,\mathbf{x}'_A,t) = \sum_i u^+(\mathbf{x}_A,\mathbf{x}_S^{(i)},t)*u^+(\mathbf{x}'_A,\mathbf{x}_S^{(i)},-t). \quad (42)$$

Note that, according to equation 41, $C(\mathbf{x}_B,\mathbf{x}'_A,t)$ is nearly identical to the correlation function of equation 1; hence, equation 41 represents the virtual-source method of Bakulin and Calvert (2004, 2006) but applied to decomposed wavefields (Mehta et al., 2007a). According to equation 42, $\Gamma(\mathbf{x}_A,\mathbf{x}'_A,t)$ contains the correlation of the incident wavefields. We call this the *point-spread function*. For equidistant sources and a homogeneous overburden, the point-spread function will approach $\Gamma(\mathbf{x}_A,\mathbf{x}'_A,t) = \delta(\mathbf{x}_A - \mathbf{x}'_A)S_s(t)$ (with $\mathbf{x}_A$ and $\mathbf{x}'_A$ both in the borehole). Hence, for this situation, equation 40 reduces to $C(\mathbf{x}_B,\mathbf{x}'_A,t) = G(\mathbf{x}_B,\mathbf{x}'_A,t)*S_s(t)$, meaning that for this situation, the correlation method gives the correct Green's function, convolved with $S_s(t)$.

For the situation of an irregular source distribution and/or a complex overburden, the point-spread function can become a complicated function of space and time. Equation 40 shows that the correlation method (i.e., Bakulin and Calvert's virtual-source method) gives the Green's function, distorted by the point-spread function. These distortions manifest themselves as an irregular radiation pattern of the virtual source and artifacts (spurious multiples) related to the one-sided illumination. The true Green's function follows by multidimensionally deconvolving the correlation function by the point-spread function. Van der Neut and Bakulin (2009) demonstrate that this indeed improves the radiation pattern of the virtual source and suppresses the artifacts.

Note that MDD can be carried out without knowing the source po-

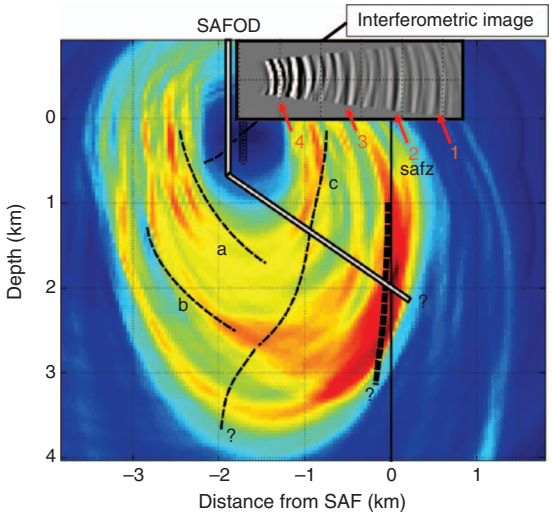

Figure 10. Images of the San Andreas Fault Observatory at depth (SAFOD). An image from deconvolution interferometry using drill-bit noise (Vasconcelos and Snieder, 2008b) is superimposed on an image obtained from surface seismic data and microseismic events from the San Andreas fault zone (SAFZ), measured at the surface and in the pilot hole (Chavarria et al., 2003). Event 2 is a prominent reflector, consistent with the surface trace of the SAF. Event 3 is interpreted to be a blind fault at Parkfield. Events 1 and 4 are interpreted to be artifacts, possibly because of drillstring multiples and improperly handled converted-wave modes.

sitions and the medium parameters (similar to crosscorrelation interferometry) and without making assumptions about the regularity of the source positions $\mathbf{x}_S^{(i)}$ and the attenuation parameters of the medium (the latter properties are unique for the deconvolution approach). The application of equations 41 and 42 requires decomposition into downgoing and upgoing waves and hence the availability of pressure and particle velocity data. The retrievable source-receiver offset range by MDD is limited by the highest velocity in the domain between the sources and the receivers. The available spatial bandwidth in the recorded data may not always be sufficient to retrieve full-range offsets. This is likely to occur in alternating velocity zones. It also occurs in areas where velocities decrease with increasing depth, which is the usual situation for electromagnetic waves (Slob, 2009).

For the situation of uncorrelated noise sources, equations 41 and 42 would need to be replaced by $C(\mathbf{x}_B,\mathbf{x}'_A,t) = \langle u^-(\mathbf{x}_B,t) * u^+(\mathbf{x}'_A, -t)\rangle$ and $\Gamma(\mathbf{x}_A,\mathbf{x}'_A,t) = \langle u^+(\mathbf{x}_A,t) * u^+(\mathbf{x}'_A, -t)\rangle$, analogous to equation 19. For a further discussion of MDD applied to passive data, see Wapenaar et al. (2008b); van Groenestijn and Verschuur (2009); and van der Neut et al. (2010).

The MDD principle is not entirely new. For example, it has been used for multiple elimination from ocean bottom data (Wapenaar and Verschuur, 1996; Amundsen, 1999; Holvik and Amundsen, 2005). Like the 1D deconvolution method of Snieder et al. (2006a) discussed above, this can be seen as a methodology that changes the boundary conditions of the system; it transforms the response of the subsurface, including the reflecting ocean bottom and water surface, into the response of a subsurface without these reflecting boundaries. In hindsight, this methodology appears to be an extension of a 1D deconvolution approach proposed by Riley and Claerbout (1976). Slob et al. (2007b) apply MDD to up/down decomposed CSEM data (Amundsen et al., 2006) and demonstrate the insensitivity to dissipation as well as the effect of changing the boundary conditions: The effect of the air wave, a notorious problem in CSEM prospecting, is largely suppressed.

Interferometry by MDD is, from a theoretical point of view, more accurate than the crosscorrelation approach; however, the involved processing is less attractive because it is not a trace-by-trace process but involves inversion of large matrices. Moreover, in most cases it requires decomposition into downgoing and upgoing fields. Nevertheless, the fact that interferometry by MDD corrects for an irregular source distribution, suppresses spurious multiples due to one-sided illumination, improves the radiation pattern of the virtual source, and accounts for dissipation makes it a worthwhile method to be investigated as an alternative to interferometry by crosscorrelation for passive and controlled-source data applications.

CONCLUSIONS

In Part 1, we discussed the basic principles of seismic interferometry in a heuristic way. In this second part, we have discussed interferometry in a more formal way. First, we reviewed the methodology of time-reversed acoustics, pioneered by Mathias Fink and coworkers, and used physical arguments of Arnaud Derode to derive seismic interferometry from the principle of time-reversed acoustics. We continued with a mathematical derivation based on general reciprocity theory leading to exact Green's function representations, which are the basis for controlled-source as well as passive interferometry. Finally, we discussed generalizations and variations of these representations and showed that those generalizations form the basis for a rich variety of new applications.

The fact that seismic interferometry leads to new responses directly from measured data has stirred a lot of enthusiasm and cooperation between researchers in seismology, acoustics, and electromagnetic prospecting in the past decennium. We believe we have only seen the start and expect to see many new developments and applications in different fields in the years to come.

ACKNOWLEDGMENTS

This work is supported by the Netherlands Research Centre for Integrated Solid Earth Science (ISES), the Dutch Technology Foundation (STW) (grant DCB.7913), and the U. S. National Science Foundation (NSF) (grant EAS-0609595). We thank associate editor Sven Treitel and reviewers Dirk-Jan van Manen, Matt Haney, and Huub Douma for their valuable comments and suggestions, which improved this paper. We are grateful to Mathias Fink, David Halliday, and Ivan Vasconcelos for permission to show the time-reversed acoustics experiment, the interferometric ground-roll removal experiment, and the interferometric SAF image, respectively.

REFERENCES

Aki, K., 1957, Space and time spectra of stationary stochastic waves, with special reference to micro-tremors: Bulletin of the Earthquake Research Institute, **35**, 415–457.
———, 1965, A note on the use of microseisms in determining the shallow structures of the earth's crust: Geophysics, **30**, 665–666.
Aki, K., and P. G. Richards, 1980, Quantitative seismology, vol. 1: W. H. Freeman & Co.
Amundsen L., 1999, Elimination of free surface-related multiples without need of the source wavelet: 69th Annual International Meeting, SEG, Expanded Abstracts, 1064–1067.
Amundsen, L., L. Løseth, R. Mittet, S. Ellingsrud, and B. Ursin, 2006, Decomposition of electromagnetic fields into upgoing and downgoing components: Geophysics, **71**, no. 5, G211–G223.
Bakulin, A., and R. Calvert, 2004, Virtual source: New method for imaging and 4D below complex overburden: 74th Annual International Meeting, SEG, Expanded Abstracts, 2477–2480.
———, 2006, The virtual source method: Theory and case study: Geophysics, **71**, no. 4, SI139–SI150.
Bakulin, A., A. Mateeva, K. Mehta, P. Jorgensen, J. Ferrandis, I. Sinha Herhold, and J. Lopez, 2007, Virtual source applications to imaging and reservoir monitoring: The Leading Edge, **26**, 732–740.
Baysal, E., D. D. Kosloff, and J. W. C. Sherwood, 1983, Reverse time migration: Geophysics, **48**, 1514–1524.
Behura, J., 2007, Virtual real source: 77th Annual International Meeting, SEG, Expanded Abstracts, 2693–2697.
Bendat, J. S., and A. G. Piersol, 2000, Random data: Analysis & measurement procedures: John Wiley & Sons, Inc.
Berkhout, A. J., 1982, Seismic migration: Imaging of acoustic energy by wave field extrapolation: Elsevier Scientific Publ. Co., Inc.
———, 1997, Pushing the limits of seismic imaging, Part I: Prestack migration in terms of double dynamic focusing: Geophysics, **62**, 937–954.
Berkhout, A. J., and D. J. Verschuur, 2001, Seismic imaging beyond depth migration: Geophysics, **66**, 1895–1912.
Berryhill, J. R., 1979, Wave-equation datuming: Geophysics, **44**, 1329–1344.
———, 1984, Wave-equation datuming before stack: Geophysics, **49**, 2064–2066.
Bojarski, N. N., 1983, Generalized reaction principles and reciprocity theorems for the wave equations, and the relationship between the time-advanced and time-retarded fields: Journal of the Acoustical Society of America, **74**, 281–285.
Brenguier, F., M. Campillo, C. Hadziioannou, N. M. Shapiro, R. M. Nadeau, and E. Larose, 2008a, Postseismic relaxation along the San Andreas fault at Parkfield from continuous seismological observations: Science, **321**, 1478–1480.
Brenguier, F., N. M. Shapiro, M. Campillo, V. Ferrazzini, Z. Duputel, O. Coutant, and A. Nercessian, 2008b, Towards forecasting volcanic eruptions using seismic noise: Nature Geoscience, **1**, 126–130.
Cao, W., G. T. Schuster, G. Zhan, S. M. Hanafy, and C. Boonyasiriwat, 2008,

Demonstration of super-resolution and super-stacking properties of time reversal mirrors in locating seismic sources: 78th Annual International Meeting, SEG, Expanded Abstracts, 3018–3022.
Chavarria, J. A., P. Malin, R. D. Catchings, and E. Shalev, 2003, A look inside the San Andreas fault at Parkfield through vertical seismic profiling: Science, **302**, 1746–1748.
Chávez-García, F. J., and F. Luzón, 2005, On the correlation of seismic microtremors: Journal of Geophysical Research, **110**, B11313-1–B11313-12.
Clapp, R. G., H. Fu, and O. Lindtjorn, 2010, Selecting the right hardware for reverse time migration: The Leading Edge, **29**, 48–58.
Curtis, A., 2009, Source-receiver seismic interferometry: 79th Annual International Meeting, SEG, Expanded Abstracts, 3655–3659.
Curtis, A., P. Gerstoft, H. Sato, R. Snieder, and K. Wapenaar, 2006, Seismic interferometry — Turning noise into signal: The Leading Edge, **25**, 1082–1092.
Curtis, A., and D. Halliday, 2010a, Directional balancing for seismic and general wavefield interferometry: Geophysics, **75**, no. 1, SA1–SA14.
———, 2010b, Source-receiver wavefield interferometry: Physical Review E, **81**, 046601.
Curtis, A., H. Nicolson, D. Halliday, J. Trampert, and B. Baptie, 2009, Virtual seismometers in the subsurface of the earth from seismic interferometry: Nature Geoscience, **2**, 700–704.
de Hoop, A. T., 1966, An elastodynamic reciprocity theorem for linear, viscoelastic media: Applied Scientific Research, **16**, 39–45.
———, 1988, Time-domain reciprocity theorems for acoustic wave fields in fluids with relaxation: Journal of the Acoustical Society of America, **84**, 1877–1882.
de Ridder, S. A. L., E. Slob, and K. Wapenaar, 2009, Interferometric seismoelectric Green's function representations: Geophysical Journal International, **178**, 1289–1304.
Derode, A., E. Larose, M. Campillo, and M. Fink, 2003a, How to estimate the Green's function of a heterogeneous medium between two passive sensors? Application to acoustic waves: Applied Physics Letters, **83**, 3054–3056.
Derode, A., E. Larose, M. Tanter, J. de Rosny, A. Tourin, M. Campillo, and M. Fink, 2003b, Recovering the Green's function from field-field correlations in an open scattering medium (L): Journal of the Acoustical Society of America, **113**, 2973–2976.
Derode, A., P. Roux, and M. Fink, 1995, Robust acoustic time reversal with high-order multiple scattering: Physical Review Letters, **75**, 4206–4209.
de Rosny, J., and M. Fink, 2002, Overcoming the diffraction limit in wave physics using a time-reversal mirror and a novel acoustic sink: Physical Review Letters, **89**, 124301-1–124301-4.
Dong, S., R. He, and G. T. Schuster, 2006, Interferometric prediction and least squares subtraction of surface waves: 76th Annual International Meeting, SEG, Expanded Abstracts, 2783–2786.
Douma, H., 2009, Generalized representation theorems for acoustic wavefields in perturbed media: Geophysical Journal International, **179**, 319–332.
Dowling, D. R., 1993, Phase-conjugate array focusing in a moving medium: Journal of the Acoustical Society of America, **94**, 1716–1718.
Draeger, C., and M. Fink, 1999, One-channel time-reversal in chaotic cavities: Theoretical limits: Journal of the Acoustical Society of America, **105**, 611–617.
Draganov, D., R. Ghose, E. Ruigrok, J. Thorbecke, and K. Wapenaar, 2010, Seismic interferometry, intrinsic losses, and Q-estimation: Geophysical Prospecting, **58**, 361–373.
Esmersoy, C., and M. Oristaglio, 1988, Reverse-time wave-field extrapolation, imaging, and inversion: Geophysics, **53**, 920–931.
Etgen, J., S. H. Gray, and Y. Zhang, 2009, An overview of depth imaging in exploration geophysics: Geophysics, **74**, no. 6, WCA5–WCA17.
Evers, L. G., and P. Siegmund, 2009, Infrasonic signature of the 2009 major sudden stratospheric warming: Geophysical Research Letters, **36**, L23808-1–L23808-6.
Fan, Y., and R. Snieder, 2009, Required source distribution for interferometry of waves and diffusive fields: Geophysical Journal International, **179**, 1232–1244.
Fink, M., 1992, Time-reversal of ultrasonic fields: Basic principles: IEEE Transactions on Ultrasonics, Ferroelectrics, and Frequency Control, **39**, 555–566.
———, 1997, Time reversed acoustics: Physics Today, **50**, 34–40.
———, 2006, Time-reversal acoustics in complex environments: Geophysics, **71**, no. 4, SI151–SI164.
Fink, M., and C. Prada, 2001, Acoustic time-reversal mirrors: Inverse Problems, **17**, R1–R38.
Fokkema, J. T., and P. M. van den Berg, 1993, Seismic applications of acoustic reciprocity: Elsevier Scientific Publ. Co., Inc.
Gajewski, D., and E. Tessmer, 2005, Reverse modelling for seismic event characterization: Geophysical Journal International, **163**, 276–284.
Glauber, R., and V. Schomaker, 1953, The theory of electron diffraction: Physical Review, **89**, 667–671.
Godin, O. A., 2006, Recovering the acoustic Green's function from ambient noise cross correlation in an inhomogeneous moving medium: Physical Review Letters, **97**, 054301-1–054301-4.
Grechka, V., and P. Dewangan, 2003, Generation and processing of pseudo-shear-wave data: Theory and case study: Geophysics, **68**, 1807–1816.
Grechka, V., and I. Tsvankin, 2002, PP + PS = SS: Geophysics, **67**, 1961–1971.
Grêt, A., R. Snieder, and J. Scales, 2006, Time-lapse monitoring of rock properties with coda wave interferometry: Journal of Geophysical Research, **111**, B03305-1–B03305-11.
Halliday, D., and A. Curtis, 2008, Seismic interferometry, surface waves and source distribution: Geophysical Journal International, **175**, 1067–1087.
———, 2009a, Generalized optical theorem for surface waves and layered media: Physical Review E, **79**, 056603.
———, 2009b, Seismic interferometry of scattered surface waves in attenuative media: Geophysical Journal International, **178**, 419–446.
———, 2010, An interferometric theory of source-receiver scattering and imaging: Geophysics, **75**, this issue.
Halliday, D. F., A. Curtis, J. O. A. Robertsson, and D.-J. van Manen, 2007, Interferometric surface-wave isolation and removal: Geophysics, **72**, no. 5, A69–A73.
Halliday, D., A. Curtis, P. Vermeer, C. L. Strobbia, A. Glushchenko, D.-J. van Manen, and J. Robertsson, 2010a, Interferometric ground-roll removal: Attenuation of scattered surface waves in single-sensor data: Geophysics, **75**, no. 2, SA15–SA25.
Halliday, D., A. Curtis, and K. Wapenaar, 2010b, Generalized PP + PS = SS from seismic interferometry: 80th Annual International Meeting, SEG, Expanded Abstracts, 4029–4033.
Hanafy, S. M., W. Cao, K. McCarter, and G. T. Schuster, 2009, Using super-stacking and super-resolution properties of time-reversal mirrors to locate trapped miners: The Leading Edge, **28**, 302–307.
Haney, M. M., 2009, Infrasonic ambient noise interferometry from correlations of microbaroms: Geophysical Research Letters, **36**, L19808-1–L19808-5.
Heisenberg, W., 1943, Die "beobachtbaren Größen" in der Theorie der Elementarteilchen: Zeitschrift für Physik, **120**, 513–538.
Holvik, E., and L. Amundsen, 2005, Elimination of the overburden response from multicomponent source and receiver seismic data, with source designature and decomposition into PP-, PS-, SP-, and SS-wave responses: Geophysics, **70**, no. 2, S43–S59.
Jakubowicz, H., 1998, Wave equation prediction and removal of interbed multiples: 68th Annual International Meeting, SEG, Expanded Abstracts, 1527–1530.
Kimman, W. P., and J. Trampert, 2010, Approximations in seismic interferometry and their effects on surface waves: Geophysical Journal International, **182**, 461–476.
Knopoff, L., and A. F. Gangi, 1959, Seismic reciprocity: Geophysics, **24**, 681–691.
Kohler, M. D., T. H. Heaton, and S. C. Bradford, 2007, Propagating waves in the steel, moment-frame Factor building recorded during earthquakes: Bulletin of the Seismological Society of America, **97**, 1334–1345.
Korneev, V., and A. Bakulin, 2006, On the fundamentals of the virtual source method: Geophysics, **71**, no. 3, A13-A17.
Kraeva, N., V. Pinsky, and A. Hofstetter, 2009, Seasonal variations of cross correlations of seismic noise in Israel: Journal of Seismology, **13**, 73–87.
Lerosey, G., J. de Rosny, A. Tourin, and M. Fink, 2007, Focusing beyond the diffraction limit with far-field time reversal: Science, **315**, 1120–1122.
Marston, P. L., 2001, Generalized optical theorem for scatterers having inversion symmetry: Applications to acoustic backscattering: Journal of the Acoustical Society of America, **109**, 1291–1295.
McMechan, G. A., 1982, Determination of source parameters by wavefield extrapolation: Geophysical Journal of the Royal Astronomical Society, **71**, 613–628.
———, 1983, Migration by extrapolation of time-dependent boundary values: Geophysical Prospecting, **31**, 413–420.
Mehta, K., A. Bakulin, J. Sheiman, R. Calvert, and R. Snieder, 2007a, Improving the virtual source method by wavefield separation: Geophysics, **72**, no. 4, V79–V86.
Mehta, K., J. L. Sheiman, R. Snieder, and R. Calvert, 2008, Strengthening the virtual-source method for time-lapse monitoring: Geophysics, **73**, no. 3, S73–S80.
Mehta, K., R. Snieder, and V. Graizer, 2007b, Extraction of near-surface properties for a lossy layered medium using the propagator matrix: Geophysical Journal International, **169**, 271–280.
Menke, W., 1989, Geophysical data analysis: Academic Press Inc..
Newton, R. G., 1976, Optical theorem and beyond: American Journal of Physics, **44**, 639–642.
Ohmi, S., K. Hirahara, H. Wada, and K. Ito, 2008, Temporal variations of crustal structure in the source region of the 2007 Noto Hanto earthquake, central Japan, with passive image interferometry: Earth, Planets and Space, **60**, 1069–1074.
Oristaglio, M. L., 1989, An inverse scattering formula that uses all the data:

Inverse Problems, **5**, 1097–1105.
Parvulescu, A., 1961, Signal detection in a multipath medium by M.E.S.S. processing: Journal of the Acoustical Society of America, **33**, 1674.
———, 1995, Matched-signal ("MESS") processing by the ocean: Journal of the Acoustical Society of America, **98**, 943–960.
Poletto, F., and B. Farina, 2008, Seismic virtual reflector — Synthesis and composition of virtual wavefields: 78th Annual International Meeting, SEG, Expanded Abstracts, 1367–1371.
———, 2010, Synthesis and composition of virtual reflector (VR) signals: Geophysics, **75**, no. 4, SA45–SA59.
Poletto, F., and K. Wapenaar, 2009, Virtual reflector representation theorem (acoustic medium): Journal of the Acoustical Society of America, **125**, no. 4, EL111–EL116.
Porter, R. P., 1970, Diffraction-limited, scalar image formation with holograms of arbitrary shape: Journal of the Optical Society of America, **60**, 1051–1059.
Ramírez, A. C., and A. B. Weglein, 2009, Green's theorem as a comprehensive framework for data reconstruction, regularization, wavefield separation, seismic interferometry, and wavelet estimation: A tutorial: Geophysics, **74**, no. 6, W35–W62.
Rayleigh, J. W. S., 1878, The theory of sound, vol. 2: Dover Publications, Inc., (Reprint 1945).
Riley, D. C., and J. F. Claerbout, 1976, 2-D multiple reflections: Geophysics, **41**, 592–620.
Roux, P., W. A. Kuperman, W. S. Hodgkiss, H. C. Song, T. Akal, and M. Stevenson, 2004, A nonreciprocal implementation of time reversal in the ocean: Journal of the Acoustical Society of America, **116**, 1009–1015.
Roux, P., K. G. Sabra, W. A. Kuperman, and A. Roux, 2005, Ambient noise cross correlation in free space: Theoretical approach: Journal of the Acoustical Society of America, **117**, 79–84.
Ruigrok, E., D. Draganov, and K. Wapenaar, 2008, Global-scale seismic interferometry: Theory and numerical examples: Geophysical Prospecting, **56**, 395–417.
Sawazaki, K., H. Sato, H. Nakahara, and T. Nishimura, 2009, Time-lapse changes of seismic velocity in the shallow ground caused by strong ground motion shock of the 2000 Western-Tottori earthquake, Japan, as revealed from coda deconvolution analysis: Bulletin of the Seismological Society of America, **99**, 352–366.
Schuster, G. T., 2009, Seismic interferometry: Cambridge University Press.
Schuster, G. T., and M. Zhou, 2006, A theoretical overview of model-based and correlation-based redatuming methods: Geophysics, **71**, no. 4, SI103–SI110.
Sens-Schönfelder, C., and U. Wegler, 2006, Passive image interferometry and seasonal variations of seismic velocities at Merapi volcano, Indonesia: Geophysical Research Letters, **33**, L21302-1–L21302-5.
Slob, E., 2009, Interferometry by deconvolution of multicomponent multi-offset GPR data: IEEE Transactions on Geoscience and Remote Sensing, **47**, 828–838.
Slob, E., D. Draganov, and K. Wapenaar, 2007a, Interferometric electromagnetic Green's functions representations using propagation invariants: Geophysical Journal International, **169**, 60–80.
Slob, E., and K. Wapenaar, 2007a, Electromagnetic Green's functions retrieval by cross-correlation and cross-convolution in media with losses: Geophysical Research Letters, **34**, L05307-1–L05307-5.
———, 2007b, GPR without a source: Cross-correlation and cross-convolution methods: IEEE Transactions on Geoscience and Remote Sensing, **45**, 2501–2510.
———, 2009, Retrieving the Green's function from cross correlation in a bi-anisotropic medium: Progress in Electromagnetics Research (PIER), **93**, 255–274.
Slob, E., K. Wapenaar, and R. Snieder, 2007b, Interferometry in dissipative media: Addressing the shallow sea problem for seabed logging applications: 77th Annual International Meeting, SEG, Expanded Abstracts, 559–563.
Snieder, R., 2006, Retrieving the Green's function of the diffusion equation from the response to a random forcing: Physical Review E, **74**, 046620-1–046620-4.
———, 2007, Extracting the Green's function of attenuating acoustic media from uncorrelated waves: Journal of the Acoustical Society of America, **121**, 2637–2643.
Snieder, R., A. Grêt, H. Douma, and J. Scales, 2002, Coda wave interferometry for estimating nonlinear behavior in seismic velocity: Science, **295**, 2253–2255.
Snieder, R., M. Miyazawa, E. Slob, I. Vasconcelos, and K. Wapenaar, 2009a, A comparison of strategies for seismic interferometry: Surveys in Geophysics, **30**, 503–523.
Snieder, R., and E. Şafak, 2006, Extracting the building response using seismic interferometry: Theory and application to the Millikan Library in Pasadena, California: Bulletin of the Seismological Society of America, **96**, 586–598.
Snieder, R., F. J. Sánchez-Sesma, and K. Wapenaar, 2009b, Field fluctuations, imaging with backscattered waves, a generalized energy theorem, and the optical theorem: SIAM Journal on Imaging Sciences, **2**, 763–776.
Snieder, R. K., and J. A. Scales, 1998, Time-reversed imaging as a diagnostic of wave and particle chaos: Physical Review E, **58**, 5668–5675.
Snieder, R., J. Sheiman, and R. Calvert, 2006a, Equivalence of the virtual-source method and wave-field deconvolution in seismic interferometry: Physical Review E, **73**, 066620-1–066620-9.
Snieder, R., E. Slob, and K. Wapenaar, 2010, Lagrangian Green's function extraction, with applications to potential fields, diffusion, and acoustic waves: New Journal of Physics, **12**, 063013-1–063013-24.
Snieder, R., K. van Wijk, M. Haney, and R. Calvert, 2008, Cancellation of spurious arrivals in Green's function extraction and the generalized optical theorem: Physical Review E, **78**, 036606.
Snieder, R., K. Wapenaar, and K. Larner, 2006b, Spurious multiples in seismic interferometry of primaries: Geophysics, **71**, no. 4, SI111–SI124.
Snieder, R., K. Wapenaar, and U. Wegler, 2007, Unified Green's function retrieval by cross-correlation: Connection with energy principles: Physical Review E, **75**, 036103-1–036103-14.
Stewart, J. L., W. B. Allen, R. M. Zarnowitz, and M. K. Brandon, 1965, Pseudorandom signal-correlation methods of underwater acoustic research I: Principles: Journal of the Acoustical Society of America, **37**, 1079–1090.
Thompson, D., and R. Snieder, 2006, Seismic anisotropy of a building: The Leading Edge, **25**, 1093.
Thorbecke, J., and K. Wapenaar, 2007, On the relation between seismic interferometry and the migration resolution function: Geophysics, **72**, no. 6, T61–T66.
Trampert, J., M. Cara, and M. Frogneux, 1993, *SH* propagator matrix and Q_S estimates from borehole- and surface-recorded earthquake data: Geophysical Journal International, **112**, 290–299.
van der Neut, J., and A. Bakulin, 2009, Estimating and correcting the amplitude radiation pattern of a virtual source: Geophysics, **74**, no. 2, SI27–SI36.
van der Neut, J., E. Ruigrok, D. Draganov, and K. Wapenaar, 2010, Retrieving the earth's reflection response by multi-dimensional deconvolution of ambient seismic noise: 72nd Conference & Technical Exhibition, EAGE, Extended Abstracts, P406.
van der Neut, J., and K. Wapenaar, 2009, Controlled-source elastodynamic interferometry by cross-correlation of decomposed wavefields: 71st Conference & Technical Exhibition, EAGE, Extended Abstracts, X044.
van Groenestijn, G. J. A., and D. J. Verschuur, 2009, Estimation of primaries by sparse inversion from passive seismic data: 79th Annual International Meeting, SEG, Expanded Abstracts, 1597–1601.
van Manen, D.-J., A. Curtis, and J. O. A. Robertsson, 2006, Interferometric modeling of wave propagation in inhomogeneous elastic media using time reversal and reciprocity: Geophysics, **71**, no. 4, SI41–SI60.
van Manen, D.-J., J. O. A. Robertsson, and A. Curtis, 2005, Modeling of wave propagation in inhomogeneous media: Physical Review Letters, **94**, 164301-1–164301-4.
———, 2007, Exact wave field simulation for finite-volume scattering problems: Journal of the Acoustical Society of America, **122**, EL115–EL121.
Vasconcelos, I., and R. Snieder, 2008a, Interferometry by deconvolution, Part 1: Theory for acoustic waves and numerical examples: Geophysics, **73**, no. 3, S115–S128.
———, 2008b, Interferometry by deconvolution, Part 2: Theory for elastic waves and application to drill-bit seismic imaging: Geophysics, **73**, no. 3, S129–S141.
Vasconcelos, I., R. Snieder, and H. Douma, 2009, Representation theorems and Green's function retrieval for scattering in acoustic media: Physical Review E, **80**, 036605-1–036605-14.
Vasconcelos, I., R. Snieder, and B. Hornby, 2008, Imaging internal multiples from subsalt VSP data — Examples of target-oriented interferometry: Geophysics, **73**, no. 4, S157–S168.
Wapenaar, K., 2004, Retrieving the elastodynamic Green's function of an arbitrary inhomogeneous medium by cross correlation: Physical Review Letters, **93**, 254301-1–254301-4.
———, 2006a, Green's function retrieval by cross-correlation in case of one-sided illumination: Geophysical Research Letters, **33**, L19304-1–L19304-6.
———, 2006b, Nonreciprocal Green's function retrieval by cross correlation: Journal of the Acoustical Society of America, **120**, EL7–EL13.
———, 2007, General representations for wavefield modeling and inversion in geophysics: Geophysics, **72**, no. 5, SM5–SM17.
Wapenaar, K., and J. Fokkema, 2006, Green's function representations for seismic interferometry: Geophysics, **71**, no. 4, SI33–SI46.
Wapenaar, K., J. Fokkema, and R. Snieder, 2005, Retrieving the Green's function in an open system by cross-correlation: A comparison of approaches (L): Journal of the Acoustical Society of America, **118**, 2783–2786.
Wapenaar, K., E. Slob, and R. Snieder, 2006, Unified Green's function retrieval by cross correlation: Physical Review Letters, **97**, 234301-1–234301-4.
———, 2008a, Seismic and electromagnetic controlled-source interferometry in dissipative media: Geophysical Prospecting, **56**, 419–434.

——–, 2010, On seismic interferometry, the generalized optical theorem and the scattering matrix of a point scatterer: Geophysics, **75**, no. 3, SA27–SA35.
Wapenaar, K., J. van der Neut, and E. Ruigrok, 2008b, Passive seismic interferometry by multidimensional deconvolution: Geophysics, **73**, no. 6, A51–A56.
Wapenaar, C. P. A., and D. J. Verschuur, 1996, Processing of ocean bottom data: Delft University of Technology Dolphin project, 6.1–6.24 (http://geodus1.ta.tudelft.nl/PrivatePages/C.P.A.Wapenaar/Daylight2/DELP_96G.pdf).
Weaver, R. L., 2008, Ward identities and the retrieval of Green's functions in the correlations of a diffuse wave field: Wave Motion, **45**, 596–604.
Whitmore, N. D., 1983, Iterative depth migration by backward time propagation: 53rd Annual International Meeting, SEG, Expanded Abstracts, 382–385.
Yao, H., and R. D. van der Hilst, 2009, Analysis of ambient noise energy distribution and phase velocity bias in ambient noise tomography, with application to SE Tibet: Geophysical Journal International, **179**, 1113–1132.
Zhang, Y., and J. Sun, 2009, Practical issues in reverse time migration: True amplitude gathers, noise removal and harmonic source encoding: First Break, **27**, no. 1, 53–59.